JGR Solid Earth

RESEARCH ARTICLE
10.1029/2018JB016281

Initial Rifting of the Lhasa Terrane from Gondwana: Insights From the Permian (~262 Ma) Amphibole-Rich Lithospheric Mantle-Derived Yawa Basanitic Intrusions in Southern Tibet

Yun-Chuan Zeng[1,2], Ji-Feng Xu[1,3], Mihai N. Ducea[2,4], Jian-Lin Chen[3,5], Feng Huang[1], and Le Zhang[3]

[1]State Key Laboratory of Geological Processes and Mineral Resources, and School of Earth Science and Resources, China University of Geosciences, Beijing, China, [2]Department of Geosciences, University of Arizona, Tucson, AZ, USA, [3]State Key Laboratory of Isotope Geochemistry, Guangzhou Institute of Geochemistry, Chinese Academy of Sciences, Guangzhou, China, [4]Faculty of Geology and Geophysics, University of Bucharest, Bucharest, Romania, [5]CAS Center for Excellence in Tibetan Plateau Earth Sciences, Beijing, China

Key Points:
- The Yawa intrusion is the first known Permian within-plate rocks for the Lhasa Terrane
- The Yawa intrusions were derived by partial melting of an amphibole-rich lithospheric mantle
- Initial rifting of Lhasa Terrane from the Gondwana began at late Middle Permian (~262 Ma)

Supporting Information:
- Supporting Information S1

Correspondence to:
J.-F. Xu,
jifengxu@cugb.edu.cn;
jifengxu@gig.ac.cn

Citation:
Zeng, Y.-C., Xu, J.-F., Ducea, M. N., Chen, J.-L., Huang, F., & Zhang, L. (2019). Initial rifting of the Lhasa Terrane from Gondwana: Insights from the Permian (~262 Ma) amphibole-rich lithospheric mantle-derived Yawa basanitic intrusions in southern Tibet. *Journal of Geophysical Research: Solid Earth*, *124*, 2564–2581. https://doi.org/10.1029/2018JB016281

Received 3 JUL 2018
Accepted 2 MAR 2019
Accepted article online 5 MAR 2019
Published online 18 MAR 2019

Abstract The Permian tectonic setting of the Lhasa Terrane in southern Tibet remains controversial (i.e., continental rift vs. subduction-collision) and is crucial to palinspastic reconstructions of the eastern Tethys during the breakup of Gondwana. In this study, we present new geochronological, geochemical, and mineralogical data for the Permian (~262 Ma) Yawa intrusions in the southern Lhasa Terrane. These rocks are silica-undersaturated and alkaline, with high TiO_2 and moderate MgO, and exhibit enrichments in Th, light rare earth elements, and Nb-Ta, and depletions in K. These chemical compositions, combined with uniform whole-rock $(^{87}Sr/^{86}Sr)_i$ (0.7039–0.7044), $\varepsilon_{Nd}(t)$ (1.85–2.81), and $\varepsilon_{Hf}(t)$ (4.21–6.90) values, and zircon $\varepsilon_{Hf}(t)$ (4.53–9.97) and $\delta^{18}O$ (5.04‰–5.76‰) values, indicate the magmas were derived by partial melting of amphibole-rich lithospheric mantle. The magmas subsequently underwent fractionation of clinopyroxene, amphibole, and Fe-Ti oxides. The amphibole in the lithospheric mantle likely formed as cumulates from low-degree asthenospheric melts during incipient extension. Given that the amphibole-rich metasomatic veins have a lower melting temperature than the surrounding peridotite, they were susceptible to melting during the early stages of thermal perturbation of the mantle. Because there is no evidence of Permian continental subsidence in the Lhasa Terrane, we suggest the Yawa intrusions were formed at the onset of lithospheric extension associated with initial rifting of the Lhasa Terrane from the Indian Plate during Gondwana breakup, which was a precursor to the opening of the Neo-Tethys Ocean.

1. Introduction

Continental rifting of Gondwana started in the early Carboniferous and peaked in the Permian, leading to the breakup of the supercontinent and opening of several Tethyan oceanic basins. The closure of these basins was accompanied by the northward assembly of Gondwana-derived terranes and formation of the Tethyan Orogenic Belt (e.g., Metcalfe, 2002, 2009, 2011, 2013). The formation of the Tibetan Plateau was a key part of this process and is generally thought to have resulted from the amalgamation of several Gondwana-derived terranes (e.g., the Qiangtang and Lhasa Terranes) or continents (e.g., the Indian Plate) with the Eurasian Plate. The successive formation and destruction of the Paleo-, Meso-, and Neo-Tethys oceanic basins in response to repeated continental rifting and collision has occurred since the Permian (Figure 1a; Cocks & Torsvik, 2013; Metcalfe, 2002, 2009, 2011, 2013; Yin & Harrison, 2000; Zhu, Zhao, Niu, Dilek, et al., 2011). However, the paleogeographic history of the Lhasa Terrane remains a key unknown in late Paleozoic paleogeographic reconstructions of eastern Asia during the breakup of the Gondwana supercontinent. Given that the Lhasa, Qiangtang, and Himalayan terranes were covered by similar Paleozoic shelf strata containing glacial diamictites and cold- to cool-water faunas, they are considered to have been connected N-S-trending segments situated on the northern passive continental margin of the Indian Plate in Gondwana, which drifted northward during the Permian-Early Triassic as the Meso- and Neo-Tethys oceans opened (e.g., Ali et al., 2013; Chen et al., 2017; Gehrels et al., 2011; Metcalfe, 2002, 2011; Yin & Harrison, 2000). However, the geochemistry of Permian igneous rocks and the detrital zircon provenance of late Paleozoic strata in the Lhasa Terrane are somewhat different to those in the

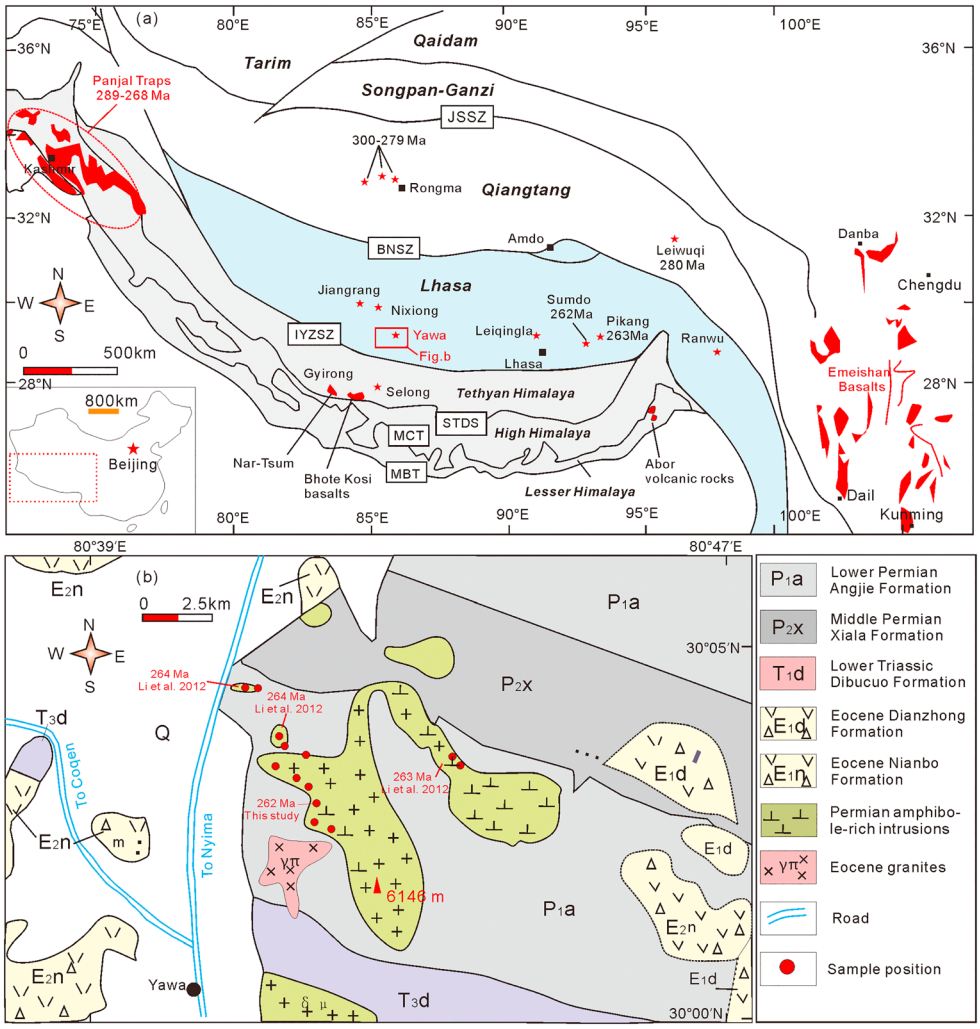

Figure 1. (a) Simplified tectonic map of the Tibetan Plateau, showing the localities of Permian volcanic rocks (after Yin & Harrison, 2000; Zhu et al., 2010) and (b) geological map of the Yawa region, southern Lhasa Terrane. Abbreviations: IYZSZ = Indus-Yarlung Zangbo Suture Zone; BNSZ = Bangong-Nujiang Suture Zone; JSSZ = Jinsha Suture Zone; MBT = Main Boundary Thrust; MCT = main central thrust; STDS = Southern Tibetan Detachment System.

Himalayan and Qiangtang terranes (arc-type vs. rift-type and detrital zircon age populations of ~1,170 vs. 950 Ma, respectively; e.g., Ferrari et al., 2008; Metcalfe, 2013; Stampfli & Borel, 2002; Zhang et al., 2013; Zhu et al., 2009, 2010; Zhu, Zhao, Niu, Dilek, et al., 2011). As such, it has been suggested that the Lhasa Terrane drifted northward from Australian parts of Gondwana and was a microcontinent within the Paleo-Tethys Ocean or part of a subduction-collision orogenic system during the Permian, whereas the Himalayan and Qiangtang terranes were the passive margin of the Indian part of Gondwana and underwent Permian rifting. These two contrasting hypotheses have significant implications for our understanding of the tectonic and paleogeographic evolution of the eastern Tethys during Gondwana breakup, particularly the timing and geodynamics of the opening of the Neo-Tethys Ocean (e.g., Metcalfe, 2011, 2013; Yin & Harrison, 2000; Zhu et al., 2013).

Paleomagnetism is a useful tool for palinspastic reconstructions. However, paleomagnetic data for Permian rocks from the Lhasa Terrane are still sparse, and the studied rocks are mostly remagnetized (Ali et al., 2013; Li et al., 2016; Xu et al., 2015). In addition, paleomagnetism can only constrain the paleolatitude of a kinematically independent plate, not its paleolongitude, and the Permian paleolatitudes of the Indian and Australian parts of Gondwana were probably similar (Li et al., 2016). Therefore, the key to resolving this issue is to identify the tectonic setting of the Lhasa Terrane (i.e., continental rift vs. subduction-collision)

in the Permian (e.g., Chen et al., 2017; Metcalfe, 2002, 2009, 2011, 2013; Yin & Harrison, 2000; Zhu et al., 2010, 2013). Although studies favoring the first model argue that the diversity of Paleozoic strata in the Lhasa Terrane does not represent robust evidence against off the northern Indian Plate (e.g., Chen et al., 2017; Gehrels et al., 2011; Jin et al., 2015), the range of igneous rocks in these terranes must be explained. However, there are few high-precision geochronological data for Permian igneous rocks in the Lhasa Terrane (Figure 1a). Thus, research into the distribution and tectonic setting of Permian igneous rocks in the Lhasa Terrane is required.

Numerous studies have revealed that mantle metasomatic phases such as amphibole or phlogopite, or veins/domains dominated by these metasomatic phases, represent an important lithology in the lithospheric mantle (e.g., Pilet, 2015; Pilet et al., 2008; Ma et al., 2011; Mayer et al., 2013; Dai et al., 2014, 2017; Ekici et al., 2014; Rooney et al., 2014, 2017; Tappe et al., 2016). Importantly, due to these metasomatic phases having a lower melting temperature than surrounding peridotite, they are susceptible to melting during the early stages of thermal perturbation of the mantle (e.g., early continental rifting). Melts generated from the amphibole-rich lithospheric mantle will have distinct geochemical characteristics (e.g., Pilet, 2015; Pilet et al., 2008, 2011). In this study, we present geochronological, geochemical, and mineralogical data for the Permian (~262 Ma) Yawa intrusions in the southern Lhasa Terrane (Figure 1b), to evaluate their mantle source characteristics and petrogenesis. The rocks in the intrusions are kaersutite bearing and basanitic to basaltic trachyandesitic in composition. The rocks have high TiO_2 contents, Nb-Ta enrichment, K depletion, positive whole-rock $\varepsilon_{Nd}(t)$ and $\varepsilon_{Hf}(t)$ values, and positive zircon $\varepsilon_{Hf}(t)$ and mantle-like zircon $\delta^{18}O$ values. These chemical and isotopic features indicate derivation by the partial melting of an amphibole-rich lithospheric mantle. Therefore, in combination with the regional geology, our study provides evidence for an extensional setting for the Lhasa Terrane in the Permian, and new constraints on the timing of initial rifting of the Lhasa Terrane from the northern margin of the Indian part of Gondwana.

2. Geological Background and Sample Petrography

The Lhasa Terrane is one of four N-S-trending tectonic units that form the Tibetan Plateau. It is bordered by the Bangong-Nujiang Suture Zone (a relic of the Meso-Tethys Ocean) to the north and the Indus-Yarlung-Tsangpo Suture Zone (a relic of the Neo-Tethys Ocean) to the south (Figure 1a; e.g., Yin & Harrison, 2000; Metcalfe, 2013; Zhu et al., 2013). The Lhasa Terrane is considered to have rifted from the Indian or Australian parts of Gondwana and then drifted northward before finally being amalgamated with the Qiangtang Terrane during the Early Cretaceous (e.g., Kapp et al., 2007; Metcalfe, 2013; Yin & Harrison, 2000; Zhu et al., 2013). The crust of the Lhasa Terrane underwent pre-Cenozoic shortening, possibly by >40%, during this collisional event (e.g., Kapp et al., 2007). It then collided with the Indian Plate during the Late Cretaceous-early Tertiary, which may have caused significant crustal thickening and uplift of the Tibetan Plateau (e.g., Chung et al., 2005; Yin & Harrison, 2000). In addition, separate crustal fragments may have amalgamated with the Lhasa Terrane prior to its collision with the Qiangtang Terrane (Figure 1a; e.g., Yang et al., 2009; Zhu, Zhao, Niu, Mo, et al., 2011). Significantly, the Sumdo oceanic eclogite of the central Lhasa Terrane, which yields protolith and metamorphic ages of ~300 and ~260 Ma, respectively, probably represents a fragment of Paleo-Tethys oceanic crust (Figure 1a; e.g., Yang et al., 2009). The Lhasa Terrane consists mainly of Paleozoic and Mesozoic marine strata and Late Triassic-early Tertiary Gangdese granitoids (e.g., Ji et al., 2009; Zhu et al., 2017). Paleozoic sedimentary strata are distributed primarily in the central-northern part of the Lhasa Terrane and comprise Carboniferous sandstones, metasandstones, shales, and phyllites with subordinate Ordovician, Silurian, and Permian limestones and interbedded mafic and silicic volcanic rocks (Gehrels et al., 2011; Yin & Harrison, 2000). The flora and fauna, glaciomarine diamictites, and detrital zircon provenance data of these Paleozoic sedimentary strata indicate that the Lhasa Terrane was located on the Indian-Australian margin of Gondwana until the early Permian (Metcalfe, 2013, and references therein). The Gangdese batholith is >3,000 km long, extending from the Chayu-western Yunnan (Dianxi)-Burma batholith in the east to the Kohistan-Ladakh batholith in the west (e.g., Ji et al., 2009; Mo et al., 2009). Pre-Mesozoic igneous rocks in this region have been the focus of several studies (e.g., Ding et al., 2015; Ji et al., 2012; Zhu et al., 2009, 2010). However, among the studied Permian igneous rocks (Figure 1a), only the Pikang granite in the central Lhasa Terrane has been dated by zircon U-Pb geochronology (Figure 1a; Zhu et al., 2009). The Pikang granite occurs as relicts of variable size or apophyses (~80 m wide) within Early Cretaceous granite that intruded Paleozoic-Jurassic sedimentary rocks.

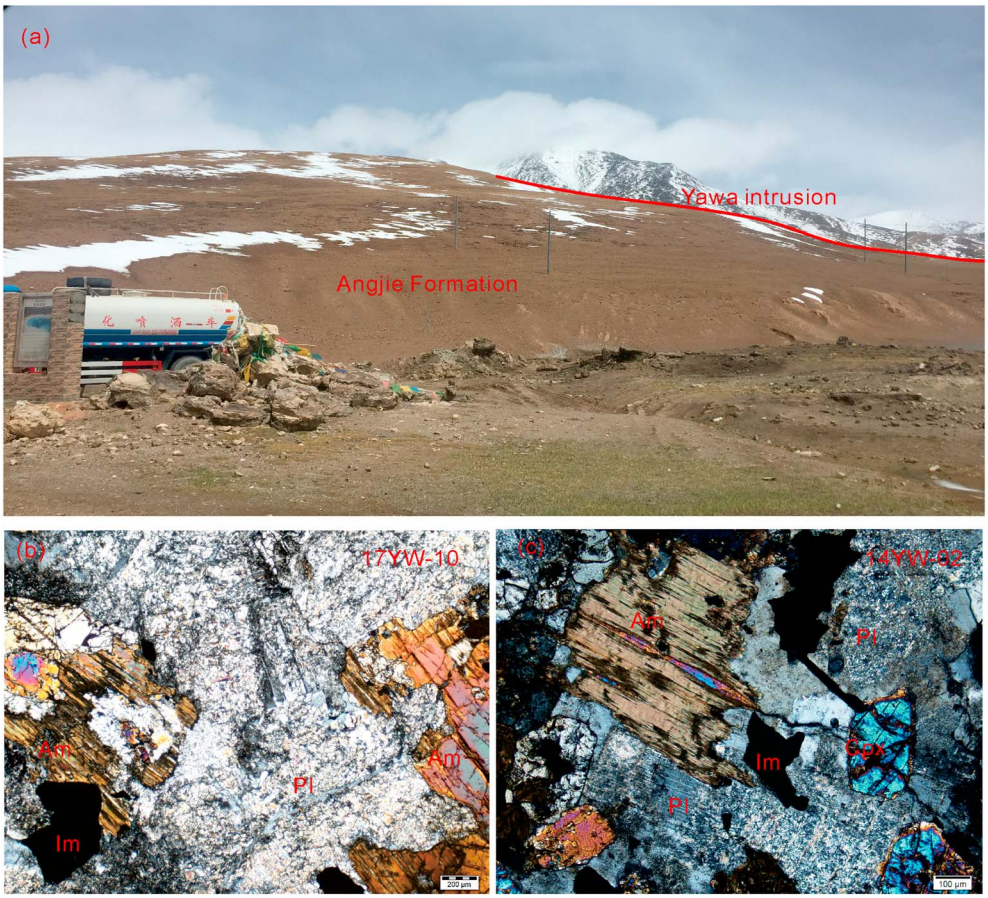

Figure 2. (a) Field site and (b and c) photomicrographs (cross-polarized light) showing the mineral composition and texture of the Yawa intrusions. Abbreviations: Am = amphibole; Im = ilmenite; Pl = plagioclase; Cpx = clinopyroxene.

These rocks show a geochemical affinity to S-type granites, including high A/CNK (≥1.08) and normative corundum (1.3%–2.0%) values and high $(^{87}Sr/^{86}Sr)_i$ (>0.708) and low $\varepsilon_{Nd}(t)$ (less than −6.0) values. Integrating these data with those for Early-Middle arc-type basalts has led to the Pikang granite being interpreted as evidence for a tectonic transition from subduction to collision in the Lhasa Terrane during the Permian (Zhu et al., 2009, 2010).

We collected samples from three intrusions located close to the village of Yawa in the southern Lhasa Terrane (Figure 1b). The samples are medium to coarse grained and consist mainly of amphibole and plagioclase, with minor clinopyroxene, apatite, ilmenite, and zircon (Figure 2). The rocks have been altered to varying degrees, whereby small amounts of amphibole and clinopyroxene have been epidotized and most of the plagioclase has been sericitized and epidotized (Figures 2b and 2c). Sedimentary strata exposed in the study area include the lower Permian Angjie, middle Permian Xiala, Upper Triassic Dibucuo, and Eocene Linzizong formations, and the rocks sampled for this study intrude the Angjie and Xiala formations (Figure 1b). The Angjie Formation in this region comprises bioclastic limestone, quartzose sandstone, and siltstone and is conformably overlain by the Xiala Formation, which comprises crinoid-bearing limestone with interbedded sandstone, mudstone, and siliceous rocks.

3. Analytical Methods and Results

Details of analytical methods for zircon U-Pb and Lu-Hf isotope analysis, whole-rock major and trace element and Sr-Nd isotope analysis, and in situ major and trace element analysis of amphibole can be found in the supporting information (Li et al., 2010; Liang et al., 2018; Liu et al., 2008, 2015; Wang et al., 2017).

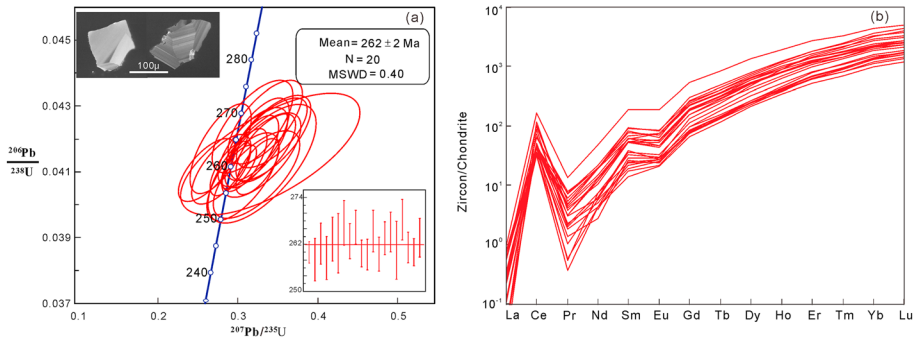

Figure 3. (a) Zircon U-Pb concordia plots and representative cathodoluminescence images of zircon grains from sample 14YW-01 and (b) chondrite-normalized rare earth element plot of the Yawa intrusion zircon grains. Normalizing values are from Sun and McDonough (1989).

3.1. Zircon U-Pb Geochronological, Trace Element, and Hf-O Isotope Data

Zircon U-Pb, trace element, and Hf-O isotope data are listed in Tables S1–S3. Twenty-four U-Pb isotopic analyses were carried out on zircon grains from sample 14YW-01. Twenty concordant analyses yielded $^{206}Pb/^{238}U$ ages of 258 ± 5 to 268 ± 6 Ma, with a weighted mean age of 262 ± 2 Ma (±2σ; mean standard weighted deviation (MSWD) = 0.4; Figure 3a). Zircon Lu-Hf isotope analyses were performed near the sites of O isotope analyses. All these analyses yielded low $^{176}Lu/^{177}Hf$ ratios (<0.003), indicating negligible radiogenic Hf in-growth after zircon formation. The Yawa zircon grains exhibit uniform $^{176}Hf/^{177}Hf$ values of 0.282436–0.282600 and age-corrected $(^{176}Hf/^{177}Hf)_i$ values of 0.282745–0.282898, yielding age-corrected $\varepsilon_{Hf}(t)$ values and Hf model ages (T_{DM}) of 4.53–9.97 and 507–729 Ma, respectively (Table S3; Figure 4a). Zircon O isotopic compositions are relatively homogeneous, with $\delta^{18}O$ values of 5.04‰ to 5.76‰ (Figure 4b; Table S3) and a mean value of 5.39‰ ± 0.17‰ (±2σ; $n = 15$), consistent with that of igneous zircon grains in equilibrium with mantle-derived magmas (5.3‰ ± 0.3‰; Valley, 2003).

The zircon grains analyzed in this study comprise whole crystals and fragments of long euhedral crystals with lengths of 100–150 μm. All crystals are relatively homogeneous, exhibiting either weak and broad or oscillatory zoning in cathodoluminescence images (Figure 3a), which is typical of zircon grains in igneous rocks (Corfu et al., 2003). In addition, the zircon grains have high Th/U ratios (≥0.5) (Table S2), strongly depleted light rare earth element (LREE) and enriched heavy rare earth element (HREE) patterns, negative Eu and positive Ce anomalies (Figure 3b), and mantle-like zircon Hf-O isotopes (Figure 4b), which further indicate a magmatic origin without recrystallization (Corfu et al., 2003; Hoskin & Black, 2000). In summary, our new age data indicate formation of the Yawa intrusions at ~262 Ma, which is consistent with the results of Li et al. (2012).

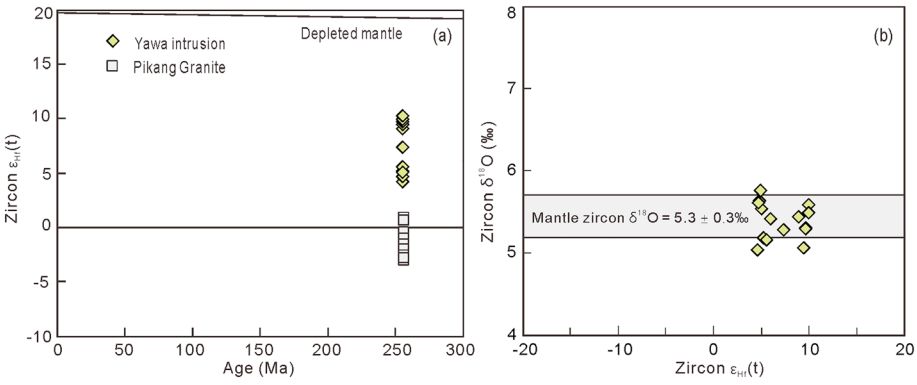

Figure 4. (a) Plots of zircon $\varepsilon_{Hf}(t)$ versus age (Ma) and (b) zircon $\varepsilon_{Hf}(t)$ versus zircon $\delta^{18}O$ for the Yawa intrusions. Zircon $\varepsilon_{Hf}(t)$ values of the Pikang granite are from Zhu et al. (2009), and mantle zircon $\delta^{18}O$ values are from Valley (2003).

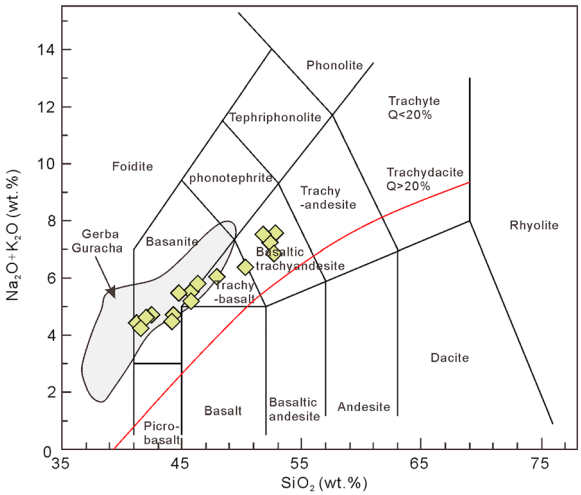

Figure 5. $Na_2O + K_2O$ versus SiO_2 diagram for the Yawa intrusions (total alkalis vs. silica diagram; Le Maitre, 2002). Data for the Gerba Guracha volcanic rocks are from Rooney et al. (2014, 2017).

3.2. Whole-Rock Major and Trace Element and Sr-Nd-Hf Isotope Data

The whole-rock major and trace element data are listed in Table S4. Major elements were recalculated and presented on an anhydrous basis in all figures. The Yawa intrusions have low SiO_2 (38.45–52.86 wt.%); high TiO_2 (2.34–4.88 wt.%), $Fe_2O_3^T$ (6.34–17.85 wt.%), and $K_2O + Na_2O$ (3.07–7.51 wt.%); and moderate MgO (3.33–8.21 wt.%) contents. Data for the intrusions are plotted within the alkaline field on the total alkalis versus silica diagram, and they are classified as sodic basanites to basaltic trachyandesites (Figure 5). In general, the major element data of the Yawa intrusions show linear trends on Harker diagrams (Figure 6).

Chondrite-normalized REE and primitive-mantle-normalized multielement diagrams are shown in Figure 7. REE patterns are steep with varying degrees of LREE enrichment relative to HREE, with $(La/Yb)_N$ ratios (where N denotes chondrite normalized) of 15.15–31.12 and $(Dy/Yb)_N$ ratios of 1.58–2.35. The primitive-mantle-normalized trace element patterns are typically steeply sloping, with enrichment of high-field-strength elements over large-ion lithophile elements, and negative K anomalies. In general, the Yawa intrusions share many similarities with typical ocean island basalts (Sun & McDonough, 1989) but have higher incompatible element concentrations.

The Yawa intrusions have a narrow range of age-corrected initial isotopic compositions (Table S5; Figure 8). They are characterized by $(^{143}Nd/^{144}Nd)_i$ values of 0.512394–0.512443 with age-corrected $\varepsilon_{Nd}(t)$ values of 1.85–2.81, $(^{87}Sr/^{86}Sr)_i$ values of 0.7039–0.7044, and $(^{176}Hf/^{177}Hf)_i$ values of 0.282748–0.282836 with age-corrected $\varepsilon_{Hf}(t)$ values of 4.53–9.97, which are mostly consistent with the zircon $\varepsilon_{Hf}(t)$ values. The end-member values used for Hf isotope calculations are from Blichert-Toft and Albarède (1997), Griffin et al. (2000), and Soderlund et al. (2004).

3.3. In Situ Amphibole Geochemistry

The studied amphibole grains are high in SiO_2 (38.29–41.23 wt.%), CaO (11.69–12.47 wt.%), MgO (10.86–12.94 wt.%), TiO_2 (5.23–6.41 wt.%), FeO (10.15–14.09 wt.%), and Al_2O_3 (11.75–13.16 wt.%) and contain minor amounts of Na_2O (2.01–2.62 wt.%) and K_2O (1.06–1.30 wt.%; Table S6). The amphibole grains are classified as kaersutite, given their high TiO_2 contents, together with their Mg and K values. This is a class of amphibole that is restricted to alkaline rocks (Figure 9a; Molina et al., 2009; Ridolfi et al., 2010). The in situ trace element data for amphibole grains of the Yawa intrusions are listed in Table S7. On a chondrite-normalized REE diagram, the amphibole data exhibit minor fractionation between the LREE and middle rare earth element ($[La/Sm]_N$ = 0.78–1.56), but significant fractionation between LREE and HREE ($[La/Yb]_N$ = 4.64–8.46) and between middle rare earth element and HREE ($[Sm/Yb]_N$ = 4.96–7.17; Figure 9b). In addition, primitive-mantle-normalized amphibole trace element data exhibit positive Ba, Sr, and Ti anomalies and negative Th, U, Pb, and Zr anomalies (Figure 9c).

4. Petrogenesis of the Yawa Intrusions

4.1. Physical Conditions During Magma Crystallization

Compositions of amphibole grains have long been used as indicators of the pressure and temperature conditions of magmatic crystallization, but most geobarometry and geothermometry methods are restricted to calc-alkaline systems with the exception of the method proposed by Ridolfi and Renzulli (2012). The crystallization pressures, temperatures, and H_2O contents for the parental magma of the Yawa intrusions in equilibrium with amphibole grains, as estimated using this method, are 387–512 MPa, 928–1013 °C, and 4.3–5.1 wt.%, respectively (Table S5). In addition, titanium contents of zircon are also sensitive to crystallization temperature (Ferry & Watson, 2007). The values of $\alpha_{SiO2} = 1$ and $\alpha_{SiO2} = 0.69$ were used in these calculations because of the presence of minor ilmenite and absence of rutile in the Yawa intrusions. This yielded

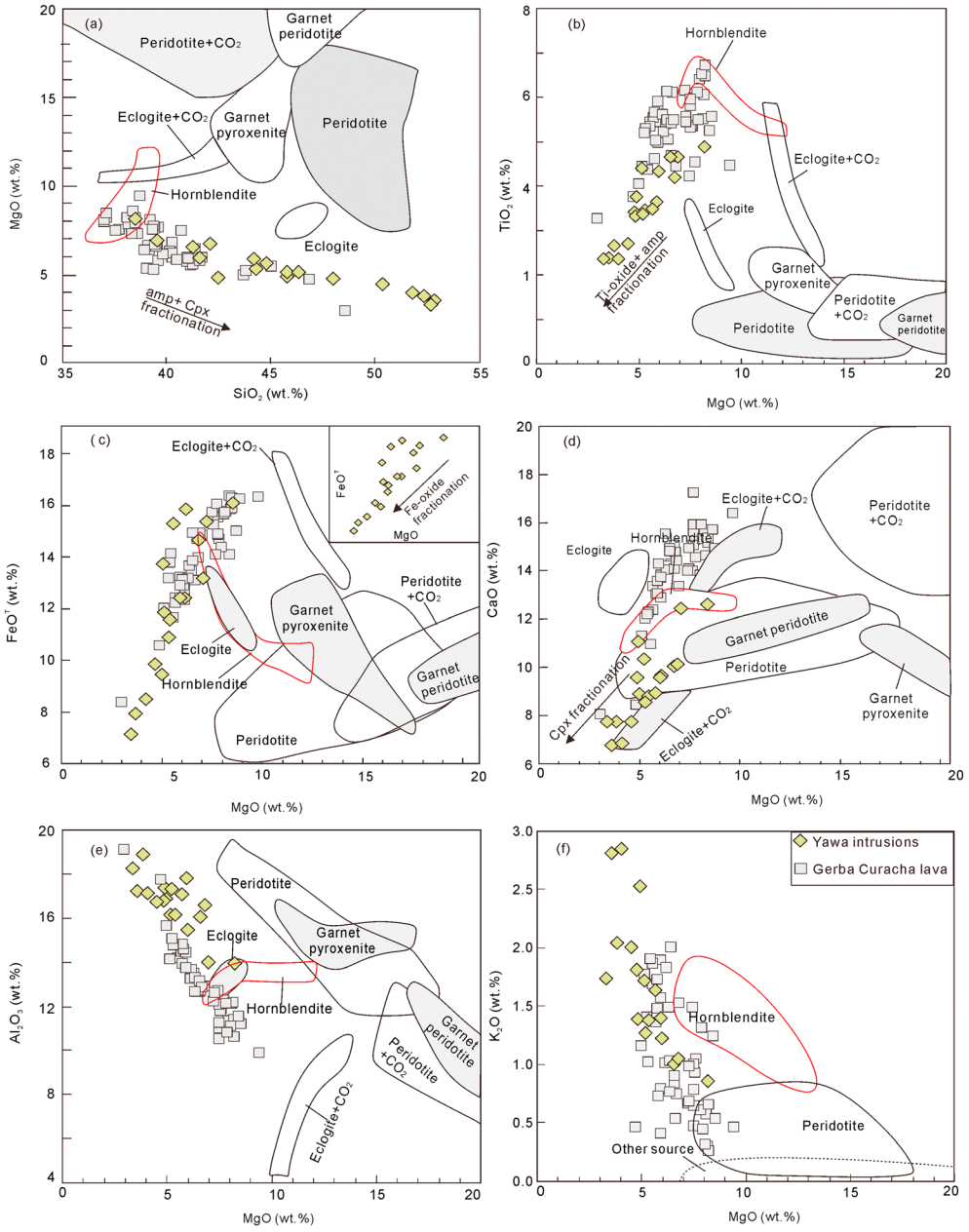

Figure 6. Harker diagrams for the Yawa intrusions. Data for the Gerba Guracha volcanic rocks are from Rooney et al. (2014, 2017), and fields for melts derived from different mantle lithologies are as follows: volatile-free peridotite (Hirose & Kushiro, 1993), garnet peridotite (Walter, 1998), peridotite + CO_2 (Dasgupta et al., 2007), dry eclogite (Kogiso & Hirschmann, 2006), carbonated eclogite (Dasgupta et al., 2006), garnet pyroxenite (Hirschmann et al., 2003), and hornblendite (Pilet et al., 2008).

temperatures of 812–969 °C, with an average of 922 °C (Table S2). These results suggest that the parental magmas of the Yawa intrusions crystallized in a high-temperature and H_2O-rich environment.

4.2. Effects of Alteration, Crustal Contamination, and Crustal Contamination

The presence of alteration minerals and variable loss-on-ignition values indicate that the rocks were altered after emplacement (Figures 2b and 2c; Table S4). The potential effects of alteration have been evaluated in Text S2 and Figure S1 (e.g., Polat et al., 2002), which shows the original concentrations of elements in the Yawa intrusions have not changed significantly during alteration, with the exception of Rb, Sr, and Ba. Therefore, these mobile elements are not considered in the discussion below.

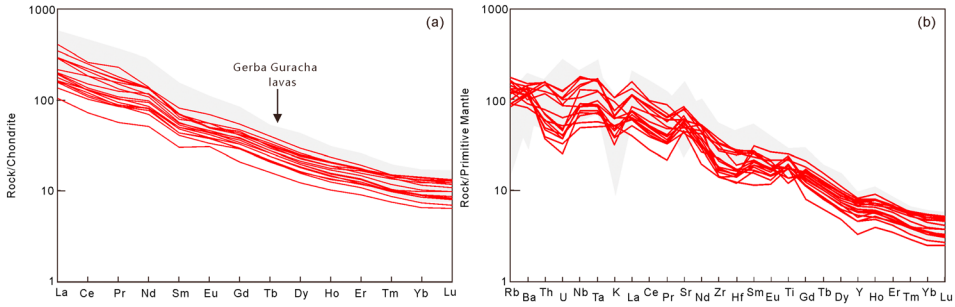

Figure 7. (a) Chondrite-normalized rare earth element and (b) primitive-mantle-normalized trace element patterns for the Yawa intrusions. Normalizing values are from Sun and McDonough (1989), and data for the Gerba Guracha volcanic rocks are from Rooney et al. (2014, 2017).

Although the Yawa intrusions were emplaced into Paleozoic sedimentary rocks (Figure 1b), we suggest that crustal contamination played a negligible role in the petrogenesis of the intrusions for several reasons. First, the Sr-Nd-Hf isotopic ratios of the intrusions are relatively uniform, whereas the Lhasa Terrane middle-upper crustal rocks, represented by the Amdo orthogneiss and Ningzhong strongly peraluminous granites, are characterized by very high $^{87}Sr/^{86}Sr$ (>0.730) and low $\varepsilon_{Nd}(t)$ (less than −7; Figure 8a; Harris et al., 1988; Liu et al., 2006; Zhu et al., 2009). Therefore, minor crustal contamination would have resulted in a marked increase in the $^{87}Sr/^{86}Sr$ values and decrease in the $\varepsilon_{Nd}(t)$ values of the Yawa intrusions, as is the case for the Panjal Traps, which were contaminated by Himalayan basement (Shellnutt, 2018; Figure 8a). Second, the Yawa intrusions have low Th/Nb and high Nb/La ratios and lack negative Nb-Ta anomalies on primitive-mantle-normalized trace element plots (Figure 7b). In addition, inherited zircon grains are absent, and the analyzed zircon grains have uniform and positive $\varepsilon_{Hf}(t)$ values (Figure 4; Table S3) and mantle-like zircon $\delta^{18}O$ values (5.04‰–5.76‰; Figure 4), which are indicative of crystallization from a homogeneous magma derived from the mantle with negligible crustal contamination (Valley, 2003).

Consequently, the considerable range in major element contents (e.g., FeO^T, Na_2O, Al_2O_3, CaO, TiO_2, and SiO_2), as well as the clear linear correlations in Harker diagrams (Figure 6), indicates that crystal fractionation is the most suitable mechanism to explain these geochemical variations. The lack of negative Eu anomalies (Figure 7a) suggests negligible fractionation of plagioclase, which may have been suppressed by the high H_2O contents of the parental magma as inferred from the amphibole compositions. The negative correlations between MgO and SiO_2, TiO_2 and SiO_2, and FeO^T and SiO_2 indicate that minerals including clinopyroxene, amphibole, and Fe-Ti oxides were fractionated from the parental magmas of the Yawa intrusions. As the fractionation of amphibole can change the silica contents and abundances of many trace elements in a residual magma, in the following discussion of the potential mantle source composition, only rocks with

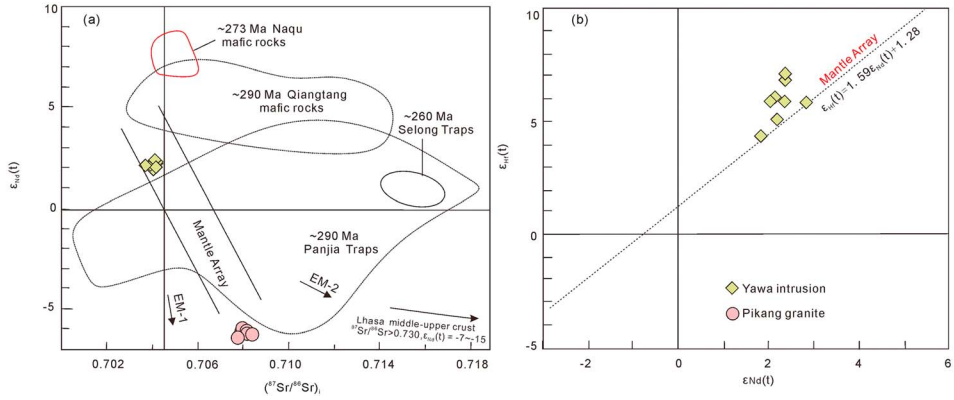

Figure 8. (a) Whole-rock $^{87}Sr/^{86}Sr_i$ versus $\varepsilon_{Nd}(t)$ and (b) $\varepsilon_{Nd}(t)$ versus $\varepsilon_{Hf}(t)$ diagrams for the Yawa intrusions. Data sources are as follows: Pikang granite from Zhu et al. (2009), Lhasa middle-upper continental crust is the Ningzhong strongly peraluminous granites and Amdo orthogneiss (Liu et al., 2006; Xu et al., 1985), ~273-Ma Naqu mafic rocks are from Chen et al. (2017), Qiangtang mafic rocks from Zhang and Zhang (2017), ~260 Ma Selong Traps from Zhu et al. (2010), Panjal traps from Shellnutt, 2018), and mantle array from Chauvel and Blichert-Toft (2001).

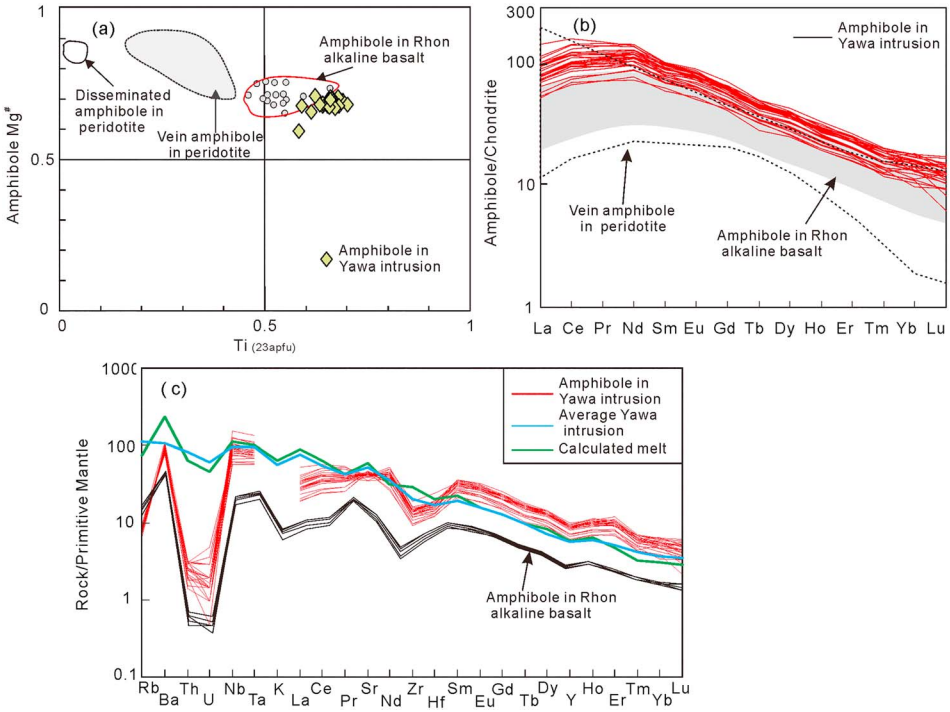

Figure 9. (a) $Mg^{\#}$ versus Ti, (b) chondrite-normalized rare earth element, and (c) primitive-mantle-normalized trace element diagrams for amphibole grains from the Yawa intrusions. Normalizing values are from Sun and McDonough (1989). Compositions of amphibole phenocrysts in the Rhon alkali basalts and vein amphibole in mantle peridotite are shown for comparison (data from Mayer et al., 2014, and references therein). The trace element concentration of melt in equilibrium with amphibole was calculated using the equation for fractional crystallization ($C_s = C_0 \times D \times F^{D-1}$). This plot only shows the calculated result using average trace element concentrations for amphibole, as given in Table S6, although data for K were determined by electron microprobe (Table S6). The Kd values of amphibole/melt vary considerably with melt composition, temperature, and pressure (see the "Geochemical Earth Reference Model" homepage; http://www.earthref.org/). To minimize this uncertainty, the Kd values for amphibole/melt used here are based mainly on experiments on a hydrous basanitic magma under a broad range of conditions (Adam & Green, 2006), apart from those of heavy rare earth elements and K that are from Bédard (2006) and Kelemen et al. (2004), respectively.

>5 wt.% MgO or >45 wt.% SiO_2, and trace element ratios that are relatively insensitive to crystal fractionation (e.g., Zr/Nb, Nb/Ta, and Zr/Hf) are considered.

4.3. Amphibole-Rich Lithospheric Mantle Composition?

The generally low SiO_2 and moderate MgO contents, coupled with the mantle-like zircon $\delta^{18}O$ values, for the Yawa intrusions suggest their magmas were derived by direct partial melting of the mantle. Specifically, the Yawa intrusion samples with relatively high MgO values are basanitic and display lower SiO_2 and MgO values than experimental melts of volatile-free peridotite (Figures 4 and 5), indicating that pure peridotitic mantle is not a suitable source (Figure 6; e.g., Hirose & Kushiro, 1993; Walter, 1998). In addition to peridotite, experiments have shown that the following mantle compositions can be the source of alkaline SiO_2-undersaturated melts: (1) silica-deficient pyroxenite-eclogite (e.g., Dasgupta et al., 2006; Hirschmann et al., 2003; Kogiso et al., 2003; Kogiso & Hirschmann, 2006; Lambart et al., 2016); (2) domains dominated by amphibole or phlogopite veins (Pilet et al., 2008); and (3) carbonated peridotite (e.g., Dasgupta et al., 2007; Hirose, 1997). Numerous experiments have shown that partial melting of silica-deficient pyroxenite-eclogite, which is either nominally anhydrous or contains CO_2, can potentially explain the low SiO_2 contents of alkaline rocks (e.g., Dasgupta et al., 2006; Keshav et al., 2004). However, such melts should have significantly lower K_2O contents (<0.2 wt.%) than those of the Yawa intrusions (Figure 6f; Dai et al., 2014, 2017; Pilet et al., 2008). Therefore, a silica-deficient pyroxenite-eclogite source cannot account for the chemical composition of the alkaline Yawa intrusions. Carbonated peridotite has been considered as another possible source for strongly SiO_2-undersaturated basalts (Dasgupta et al., 2007). However, melts derived from carbonated peridotite are characterized by high CaO/Al_2O_3, Zr/Hf, and Nb/Ta (Figures 10a

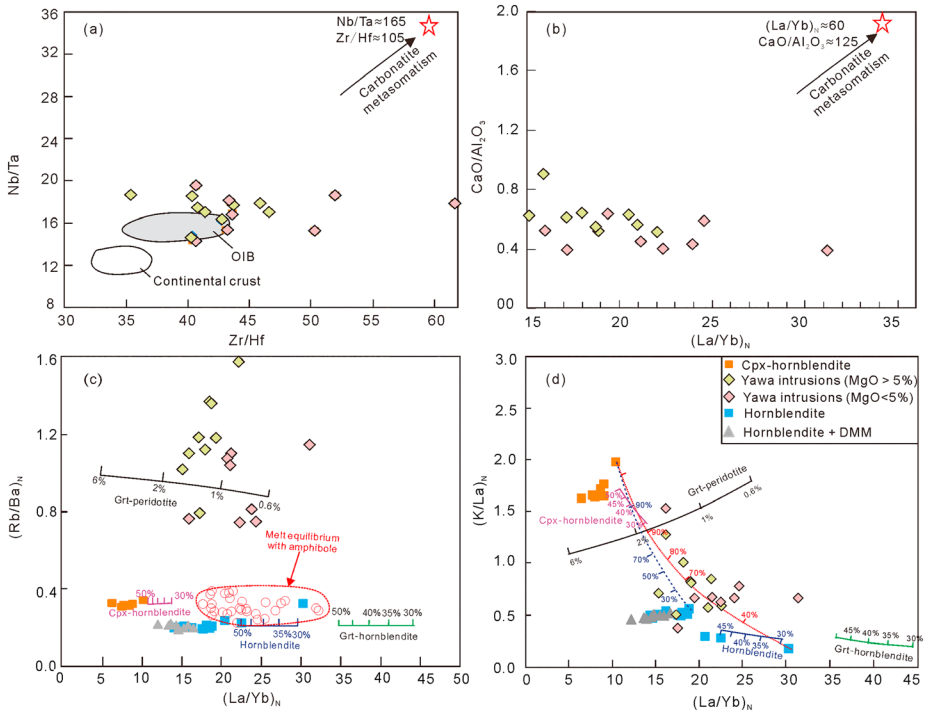

Figure 10. (a) Zr/Hf versus Nb/Ta, (b) La/Yb versus CaO/Al_2O_3, (c) $(La/Yb)_N$ versus $(Rb/Ba)_N$, and (d) $(La/Yb)_N$ versus $(K/La)_N$ diagrams for the Yawa intrusions, showing the features of the source rocks. The red five-pointed stars in (a) and (b) are representative of the composition of average carbonatites from Hoernle et al. (2002) and Bizimis et al. (2003). In (c) and (d), the data for hornblendite, cpx-hornblendite, and hornblendite + DMM (depleted mantle) are from Pilet et al. (2008). The forward modeling results of these lithologies are shown for comparison, which generally overlap with the experimentally determined values, apart from the higher $(La/Yb)_N$ values of garnet-involved melting. The modal and melting proportions, and partition coefficients used in the partial melting forward modeling, are summarized in Table S8. DMM = depleted mantle.

and 10b), and low TiO_2 (<1.5 wt.%) and K_2O (<0.2 wt.%) contents, which are not observed for the Yawa intrusions (Table S4).

In fact, peridotite with a primitive mantle composition is too depleted in TiO_2 to account for the high TiO_2 contents of most alkaline basalts (Prytulak & Elliott, 2007), and the breakdown of Ti-rich minerals (e.g., amphibole and/or phlogopite) in the mantle may be necessary to generate high-TiO_2 melts. An amphibole and/or phlogopite-bearing source can also account for the characteristic K depletion with respect to primitive mantle (Figure 7b; Furman & Graham, 1999; Späth et al., 2001). The abundant amphibole and calculated melt H_2O contents also indicate that "wet melting" of an enriched mantle domain with abundant hydrous mineral phases occurred during formation of the Yawa magmas. The low MgO contents of mafic alkaline rocks (e.g., the Yawa intrusions) are not solely the result of crystal fractionation but may also indicate the involvement of hydrous-mineral-bearing nonperidotitic sources (e.g., Foley et al., 1999; Mayer et al., 2013; Pilet et al., 2008; Figure 6). Melting of mantle containing phlogopite will result in potassic and ultrapotassic magmas with elevated Rb/Ba ratios, whereas sodic magmas with low Rb/Ba ratios are likely to form by the partial melting of amphibole-bearing mantle (e.g., Furman & Graham, 1999; Pang et al., 2015; Rosenthal et al., 2009). The high Na_2O/K_2O ratios (1.18–4.28; Table S4) of the Yawa intrusions would appear to reflect derivation from amphibole-rich lithospheric mantle, whereas the high Rb/Ba ratios are possibly indicative of phlogopite in the source. However, it must be noted that the original Rb and Ba abundances of the Yawa intrusions have been modified by alteration (Text S2; Figure S1). Instead, melts calculated to be in equilibrium with amphibole have lower Rb/Ba ratios, consistent with the melting of amphibole-bearing mantle (Figures 9c and 10c). This petrogenetic model is further supported by the similarity in geochemical compositions of experimental melts of amphibole-rich lithologies (Figures 5, 9c, and 9d), the amphibole-bearing lithospheric-mantle-derived Gerba Guracha volcanic rocks from the western Ethiopian Plateau, and the Yawa intrusions (Figure 4–6); Rooney et al., 2014, 2017). However, some of

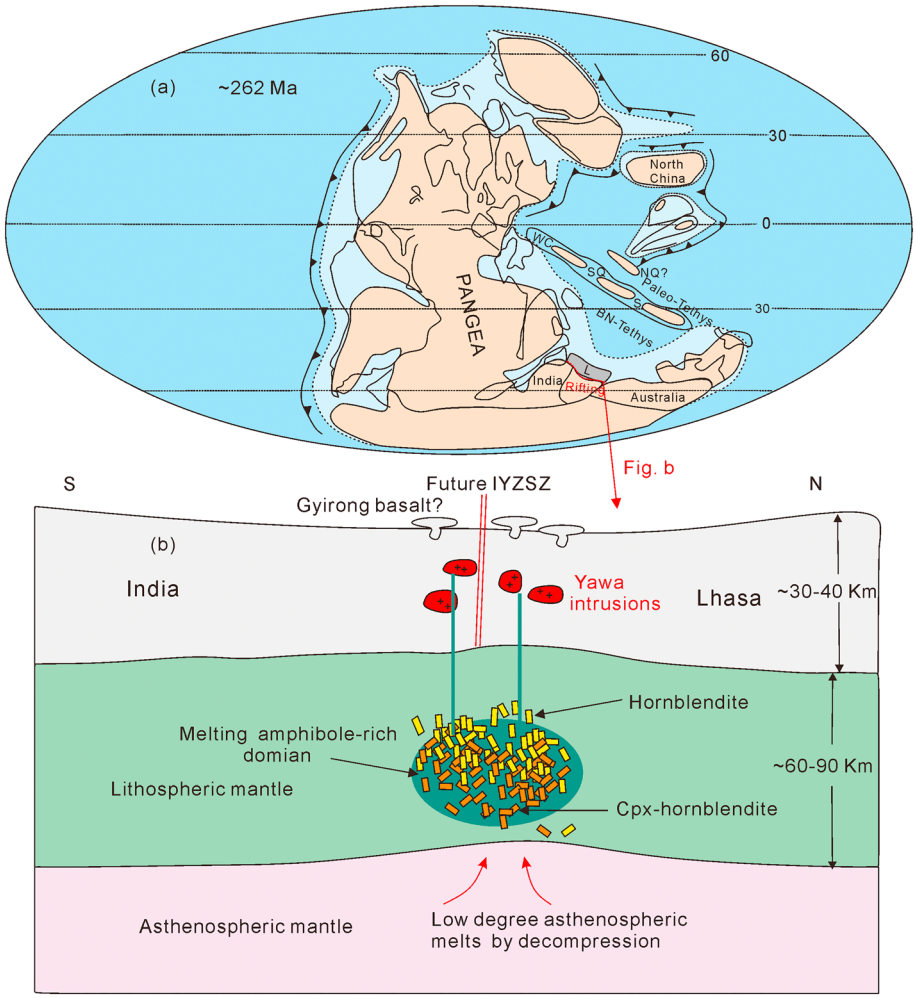

Figure 11. (a) Paleogeographic reconstruction showing the locations of Asian continental blocks on the Gondwana margin during the late-middle Permian (modified from Metcalfe, 2011, 2013). (b) Schematic illustration of the geodynamic setting of the Yawa intrusions. Abbreviations: WC = Western Cimmerian; NQ = North Qiangtang; SQ = South Qiangtang; L = Lhasa; S = Sibumasu; IYZSZ = Indus-Yarlung-Zangbo Suture Zone.

the Yawa samples have obviously higher $(K/La)_N$ ratios than pure hornblendite-derived melts (Figure 10d), which might have resulted from mixing with low-degree melts of surrounding peridotite (e.g., Dai et al., 2014; Ma et al., 2011). However, this hypothesis is unlikely because the required proportion of peridotite-derived melt is too high (up to 90%; Figure 10d). Both experimental studies and natural mantle xenoliths show that clinopyroxene-rich hornblendite (Cpx-hornblendite) is an important lithology that forms during mantle metasomatism (e.g., Pilet et al., 2008, 2011). Cpx-hornblendite-derived melt will have a similar major and trace element composition to pure hornblendite-derived melt, apart from the K/La ratio (Pilet et al., 2008; Figure 10d). A binary mixing model using experimental data for pure hornblendite and cpx-hornblendite can account for the $(K/La)_N$ variations of the Yawa intrusions (Figure 10d). In this case, the melting must have occurred in the lithospheric mantle (Figure 11), as it has been shown experimentally that amphibole is only stable at temperatures of 970–1170 °C and pressures of 1–3 GPa and thus does not exist in the convecting asthenospheric mantle (e.g., Frost, 2006; Green et al., 2010).

4.4. Formation of the Amphibole-Rich Lithospheric Mantle

Amphibole in the lithospheric mantle can be formed by the interaction of melts-fluids percolating through preexisting peridotitic lithospheric mantle (disseminated) or as cumulates from these melts-fluids (veins). The melts-fluids may be related to paleo-subduction events (e.g., Dai et al., 2014, 2017; Rooney et al., 2014; Tappe et al., 2016; Zheng, 2012) or low-degree asthenospheric melting during incipient thermal

perturbation of the mantle (e.g., Pilet, 2015). Amphibole that forms by the two mechanisms generally has the same major element composition (e.g., Mayer et al., 2014; Pilet, 2015; Pilet et al., 2008, 2011), but amphibole that precipitates in veins cutting peridotites has lower $Mg^{\#}$ values than amphibole disseminated in peridotite as intergranular minerals (Figure 9a; Soder et al., 2016, and references therein). Low-$Mg^{\#}$ amphibole preferentially incorporates Nb over Zr and Zr over Hf, leading to lower Zr/Nb and higher Zr/Hf ratios in vein assemblages (Tiepolo et al., 2001). In addition, low-$Mg^{\#}$ amphibole has similar Nb and Ta partition coefficients ($D_{Nb/Ta} \sim 1$). As the composition of the melt derived from a metasomatic mantle lithology would be controlled mainly by amphibole composition (e.g., Molina et al., 2009; Pilet et al., 2008, 2011; Rooney et al., 2014, 2017), the low MgO, $Mg^{\#}$, Zr/Nb, and Nb/Ta values; high Zr/Hf values; and chondritic Nb/Ta ratios for the Yawa intrusions are indicative of low-$Mg^{\#}$ amphibole of cumulate origin in the mantle source.

The estimated model ages of the Yawa intrusions based on whole-rock Nd-Hf and zircon Hf isotopic data are 850–500 Ma. This was a significant period in the assembly of Gondwana. If the amphibole was formed by the percolation of paleo-subduction-related melts-fluids into the lithospheric mantle at this time, their presence within the mantle for an extended period would require the melts-fluids to have existed in a stable region. This is plausible, as the early Ordovician was a period of tectonic quiescence (i.e., no thermal anomalies or extension; Metcalfe, 2013). However, given that slab-derived fluids-melts interacting with mantle peridotite are generally chromatographic in nature (e.g., Shaw et al., 2007; Stein et al., 1997) and there is greater fractionation of Lu/Hf than Sm/Nd ratios relative to the source in amphibole-rich cumulates (Pilet et al., 2011), an extended time period would result in Hf-Nd isotope decoupling, as observed in some mantle xenoliths and amphibole-rich mantle rocks (e.g., Rooney et al., 2014; Tappe et al., 2016). This is not observed for the Yawa intrusions (Figure 9b). Therefore, we suggest that the amphiboles in the mantle source of the Yawa intrusions were cumulates from low-degree asthenospheric melts in the lithospheric mantle.

5. Implications

5.1. Continental-Rift Extensional Setting for the Lhasa Terrane During the Permian?

Globally, Permian magmatism was predominantly intraplate volcanism related to mantle plume activity and the breakup of Gondwana (e.g., Shellnutt, 2018), but there is an ongoing debate as to the Permian tectonic setting of the Lhasa Terrane. The Qiangtang and Lhasa terranes are traditionally regarded as having been connected and aligned N-S and drifted northward from the northern passive margin of the Indian Plate during the Permian-Triassic, which led to the opening of the Meso- and Neo-Tethys oceanic basins, respectively (e.g., Chen et al., 2017; Gehrels et al., 2011; Metcalfe, 2002, 2011; Yin & Harrison, 2000). However, studies of Permian igneous rocks have led some researchers to suggest that the Lhasa Terrane was part of a subduction-collision orogenic system during the Permian, whereas the Himalayan and Qiangtang terranes were in a continental rift extensional setting at this time (Stampfli & Borel, 2002; Zhu et al., 2009, 2010, 2013). According to this hypothesis, the Lhasa Terrane had either drifted away before the Permian and was an isolated microcontinent within the Paleo-Tethys Ocean (Ran et al., 2012; Yang et al., 2009; Zhu et al., 2009, 2010) or part of a subduction-collision system situated along the active margin of the northern Australian Plate during the Permian to Early Triassic (Metcalfe, 2013; Zhu et al., 2009, 2010). Further evidence for the microcontinent hypothesis includes the discovery of relict Paleo-Tethys oceanic lithosphere represented by the late Carboniferous-Permian Sumdo oceanic eclogite in the Lhasa Terrane (Figure 1a; Chen et al., 2009; Yang et al., 2009), paleomagnetic data for lower Permian strata showing that the Lhasa Terrane drifted from the Southern to Northern Hemisphere rather than staying attached to the northern margin of Gondwana (Ran et al., 2012), and the biostratigraphic differences between Paleozoic sedimentary strata in the Lhasa and Himalayan terranes (Zhang et al., 2013). However, irrespective of the actual tectonic setting, we favor that the Lhasa Terrane was attached to the northern margin of Gondwana (close to the Indian or Australian plate) in the Permian for the following reasons. First, the diagnostic features of the Gondwana supercontinent (i.e., glacial diamictites and cold- or cool-water faunas) are present in the early Permian strata of the Lhasa, Qiangtang, and Himalayan terranes. Moreover, the stratigraphy and detrital zircon provenance of these strata are generally similar in all cases (Fan et al., 2017; Gehrels et al., 2011; Jin et al., 2015; Metcalfe, 2002, 2011, 2013). The presence of both cold- and warm-water fauna in the Lhasa Terrane was potentially a result of climate change (e.g., Fielding et al., 2008; Isbell et al., 2012; Jin et al., 2015). Second, the Permian pole of the Lhasa Terrane remains uncertain because the relevant

paleomagnetic data are sparse and the studied rocks are generally remagnetized (e.g., Ali et al., 2013; Xu et al., 2015). In fact, high-precision paleomagnetic data for Early Jurassic volcanic-sedimentary rocks in the southern Lhasa Terrane suggest it drifted away from Gondwana during the Triassic rather than the Permian (Li et al., 2016, and references therein). This is consistent with the occurrences of exotic Permian limestone from the Lhasa Terrane in Triassic sedimentary rocks within the Indus-Yarlung-Tsangpo Suture Zone, hinting that separation of the Lhasa Terrane from Gondwana occurred from the late Permian to Triassic. Third, field observations indicate that the Sumdo eclogite is probably not autochthonous (Gehrels et al., 2011; Zhang & Tang, 2009).

Although the arc-type geochemical features of Permian basaltic rocks in the Lhasa Terrane are possibly in contrast to those with rift-type features in the Himalayan and Qiangtang terranes, the Permian rocks in previous studies lack high-quality geochronological constraints (Figure 1a; Zhu et al., 2010). Notably, recent 1:50,000 geological mapping has revealed that the Permian Nixiong (Dibucuo) and Jiangrang mafic rocks are late-stage intrusions, rather than being interlayered with lower-middle Permian sedimentary strata (Chengdu Institute of Geology and Mineral Resources (CIGMR), 2017). In addition, the petrographic characteristics (i.e., biotite-rich with alkali feldspar megacrysts), zircon ε_{Hf} values (−4.5 to +1.9), and occurrence (i.e., xenoliths in Early Cretaceous granites; Figure 4a; Zhu et al., 2009) of the Pikang granites differ from those expected for S-type granites. Rocks with these features are more likely to have been derived by partial melting of sedimentary rocks, triggered by underplated mantle-derived rocks, and can form in various tectonic settings. Therefore, combined with the rare ~300- to 260-Ma detrital zircon grains in the Permian-Triassic sedimentary rocks of the Lhasa Terrane (Fan et al., 2017; Gehrels et al., 2011; Li et al., 2014), there is no solid evidence from Permian igneous rocks for a subduction-collisional setting for the Lhasa Terrane during the middle-late Permian.

The Yawa intrusions investigated in this study are the only confirmed Permian mafic igneous rocks in the Lhasa Terrane, which can shed further light on the tectonomagmatic evolution of this region. Their kaersutite-bearing, alkaline, ocean island basalt-type geochemical characteristics and high crystallization temperatures are evidence for intraplate volcanism during this period (Figures 1, 4, and 6); Tables S2 and S6). Despite the low solidus temperatures of hydrous metasomatic veins, lithospheric extension or a heat source is still required to trigger partial melting. Thus, the formation of continental basanitic rocks is related mainly to continental rifting, mantle plumes, and upwelling asthenosphere caused by orogenic collapse or lithospheric delamination in a post-collisional environment but is extremely rare in arcs (e.g., Dai et al., 2014; Ma et al., 2011; Mayer et al., 2014; Pang et al., 2015; Pilet, 2015; Rooney et al., 2014, 2017). The asthenospheric mantle or deep mantle plume needs to upwell sufficiently to melt at high degrees, if partial melting of the Lhasa lithospheric mantle was triggered by heating, because the amphibole in the source of the Yawa magmas requires melting at shallow levels (e.g., Frost, 2006; Green et al., 2010). However, the limited Permian intraplate volcanic rocks, and particularly the absence of asthenospheric melts in the Lhasa Terrane, indicate the Yawa intrusions were generated without much thermal perturbation (e.g., Ma et al., 2011). The relatively "cold" melting scenario is consistent with the formation mechanism of amphibole in our petrogenetic model. In addition, the continuous limestone-dominant deposition during the whole Permian in the Lhasa Terrane indicates no crustal uplift (e.g., Jin et al., 2015; Wu et al., 2014, 2017; Xie et al., 2010; Zhang et al., 2014), which would be expected in postcollisional extensional and mantle plume settings. Moreover, there is a transition from limestone-dominant Permian strata to thick clastic Early Triassic strata, reflecting the development of a rift-related basin at a passive margin (Jin et al., 2015; Wu et al., 2014, 2017; Yin & Harrison, 2000). Furthermore, rare ~300- to 260-Ma detrital zircon grains in the Permian-Triassic sedimentary rocks of the Lhasa Terrane would be expected for a continental rift setting. Therefore, we propose that the formation of the Yawa intrusions was related to passive extension of the continental lithosphere of the Lhasa Terrane.

5.2. Initial Rifting of the Lhasa Terrane From the Northern Margin of Gondwana

The Lhasa Terrane was in a continental rift setting during the late middle Permian, which is in contrast to the active margin of northern Australia at this time, where abundant Permian arc-type volcanic rocks were erupted and a tectonic unconformity formed between late Permian and Triassic sedimentary strata (e.g., Crowhurst et al., 2004; Hill & Hall, 2003; Metcalfe, 2013; Zhu et al., 2013). Therefore, it would appear to be more appropriate to place the Lhasa Terrane in the Permian-Early Triassic rift-drift system on the northern margin of the Indian Plate in the Gondwana supercontinent (Figure 11a), particularly given that the rift-

related igneous rocks and structures in the northern Australian Plate formed mainly during the Late Jurassic (Ali et al., 2013; Crowhurst et al., 2004). This hypothesis is possibly inconsistent with the different Proterozoic detrital zircon age populations observed in Paleozoic sedimentary strata in the Lhasa (~1,170 Ma) and Qiangtang-Himalayan terranes (~950 Ma), suggesting that the Lhasa Terrane drifted away from the Australian Plate rather than the Indian Plate (e.g., Zhu, Zhao, Niu, Dilek, et al., 2011). However, among the Gondwana-derived terranes or plates, the Australian Plate is not a unique source for the distinct ~1,170-Ma detrital zircon population found in Paleozoic strata of the Lhasa Terrane, which could have also been sourced from East African orogenic belts before and during the assembly of Gondwana (e.g., Zeng et al., 2018; Zhang et al., 2012). This view is supported by a recent study revealing that Permian strata in the Lhasa Terrane contains both ~950- and ~1,170-Ma detrital zircon populations (Fan et al., 2017).

More importantly, conditions for the formation of the Yawa intrusions in the Lhasa Terrane at this time include the low melting temperature of the amphibole-rich lithospheric mantle, as inferred from the amphibole thermobarometer and whole-rock geochemistry. These data, in combination with the lack of evidence for significant continental subsidence or uplift during the middle-late Permian (e.g., Wu et al., 2017; Zhang et al., 2014), indicate limited extension of the continental lithosphere during this period. Therefore, we suggest the Yawa intrusions formed due to initial rifting of the lithospheric mantle (Figure 11b). Partial melting would have facilitated lithospheric rifting, which may have gradually led to the breakup of the Lhasa Terrane, its drift away from Gondwana, and opening of the Neo-Tethys Ocean during the Early-Middle Triassic, as inferred from paleomagnetic studies (Li et al., 2016; references therein) and the presence of 212- to 237-Ma arc-type igneous rocks in the southern Lhasa Terrane (Wang et al., 2016). However, rift-related igneous rocks in the Himalayan Terrane that formed in response to the opening of the Tethys Ocean were generated mainly during the early Permian, although only the Panjal Traps have been confirmed to be of this age by zircon U-Pb dating (Figure 1a; Shellnutt, 2018; Zhu et al., 2010). Rift-related rocks associated with the drift of the Qiangtang Terrane from the northern margin of the Indian Plate were also formed during the early Permian (~300–279 Ma; Figure 1a; Zhang & Zhang, 2017, and references therein), which is consistent with paleomagnetic data (e.g., Song et al., 2017). Thus, the age distribution of rift-related rocks appears to be inconsistent with the successive separation of the N-S-connected Qiangtang and Lhasa terranes from the Indian part of Gondwana. We suggest that the formation of the Panjal Traps and Abor volcanic rocks had no geodynamic relationship with the drift of the Lhasa Terrane (Ali et al., 2013; Metcalfe, 2002; Shellnutt, 2018) or that the Lhasa and Qiangtang terranes were located along-strike from each other rather than being "stacked" against northern Great India as proposed by Wopfner and Jin (2009). In summary, the Yawa intrusions provide robust evidence of an extensional tectonic setting for the Lhasa Terrane during the Permian, which was then part of a continental rift system associated with the breakup of Gondwana. Our study supports the proposal that the Qiangtang Terrane drifted earlier than the Lhasa Terrane from the northern margin of Gondwana, which led to the successive opening of the Meso- and Neo-Tethys oceans, respectively (Figure 11; e.g., Gehrels et al., 2011; Metcalfe, 2011; Song et al., 2017; Yin & Harrison, 2000; Zhang & Zhang, 2017).

6. Conclusions

The Yawa intrusions were formed at ~262 Ma. This is the first reliably dated example of Permian mafic magmatism within the Lhasa Terrane. These intrusions show geochemical characteristics of SiO_2-undersaturated alkaline rocks derived by partial melting of amphibole-rich lithospheric mantle that subsequently underwent extensive crystal fractionation. These new data and the regional geology provide evidence for a continental rifting setting in the Permian and derivation of the Lhasa Terrane from the northern margin of the Indian Plate during Gondwana breakup. Given that amphibole-rich lithospheric mantle is susceptible to melting during the early stages of thermal perturbation of the mantle, we suggest that the Yawa intrusions were formed at the onset of lithospheric extension associated with initial rifting of the Lhasa Terrane from Gondwana, which was the precursor to the opening of the Neo-Tethys Ocean.

Acknowledgments
We thank Ying Liu, Xiang-Lin Tu, Sheng-Lin Sun, Ding-Shuai Xue, Yong-Hai Yuan, Qing Yang, and Fang-Yue Wang for the geochemical analyses and Ming Lei and Qiu-Wei Xiong for assistance with fieldwork. We are grateful for the constructive reviews by Kwan-Nang Pang and an anonymous reviewer and the encouragement and editorial support of Michael Walter and John Lassiter. This research was supported by the following funding agencies: The National Key Research and Development Project of China (project 2016YFC0600304), the Major State Basic Research Program of the People's Republic of China (2015CB452602), and the Natural Science Foundation of China (41730427, 41803030 and 41873037). M. N. Ducea acknowledges a US National Science Foundation grant (EAR 1725002) and the Romanian Executive Agency for Higher Education, Research, Development and Innovation Funding projects PN-III-P4-ID-PCE-2016-0127 and PN-III-P4-ID-PCCF-2016-0014. Supporting data are included in a supporting information file and can be obtained from the corresponding author, Ji-Feng Xu (jifengxu@cugb.edu.cn or jifengxu@gig.ac.cn).

References

Adam, J., & Green, T. (2006). Trace element partitioning between mica-and amphibole-bearing garnet lherzolite and hydrous basanitic melt: 1. Experimental results and the investigation of controls on partitioning behaviour. *Contributions to Mineralogy and Petrology*, *152*(1), 1–17. https://doi.org/10.1007/s00410-006-0085-4

Ali, J. R., Cheung, H. M., Aitchison, J. C., & Sun, Y. D. (2013). Palaeomagnetic reinvestigation of Early Permian rift basalts from the Baoshan Block, SW China: Constraints on the site-of-origin of the Gondwana-derived eastern Cimmerian terranes. *Geophysical Journal International*, *193*(2), 650–663. https://doi.org/10.1093/gji/ggt012

Bédard, J. H. (2006). A catalytic delamination-driven model for coupled genesis of Archaean crust and sub-continental lithospheric mantle. *Geochimica et Cosmochimica Acta*, *70*(5), 1188–1214. https://doi.org/10.1016/j.gca.2005.11.008

Bizimis, M., Salters, V. J. M., & Dawson, J. B. (2003). The brevity of carbonatite sources in the mantle: Evidence from Hf isotopes. *Contributions to Mineralogy and Petrology*, *145*(3), 281–300. https://doi.org/10.1007/s00410-003-0452-3

Blichert-Toft, J., & Albarède, F. (1997). The Lu-Hf geochemistry of chondrites and the evolution of the mantle-crust system. *Earth and Planetary Science Letters*, *148*, 24–258.

Chauvel, C., & Blichert-Toft, J. (2001). A hafnium isotope and trace element perspective on melting of the depleted mantle. *Earth and Planetary Science Letters*, *190*(3-4), 137–151. https://doi.org/10.1016/S0012-821X(01)00379-X

Chen, S., Yang, J., Li, Y., & Xu, X. (2009). Ultramafic blocks in Sumdo region, Lhasa block, Eastern Tibet plateau: An ophiolite unit. *Journal of Earth Science*, *20*(2), 332–347. https://doi.org/10.1007/s12583-009-0028-x

Chen, S. S., Shi, R. D., Fan, W. M., Gong, X. H., & Wu, K. (2017). Early Permian mafic dikes in the Nagqu area, central Tibet, China, associated with embryonic oceanic crust of the Meso-Tethys Ocean. *Journal of Geophysical Research: Solid Earth*, *122*, 4172–4190. https://doi.org/10.1002/2016JB013693

Chengdu Institute of Geology and Mineral Resources (CIGMR). (2017). The special report of regional geological survey of the People's Republic of China. Tectonic evolution and metallogenesis in northern Tibet (1:50000)–Cuoqin town, 1–128.

Chung, S. L., Chu, M. F., Zhang, Y., Xie, Y., Lo, C. H., Lee, T. Y., et al. (2005). Tibetan tectonic evolution inferred from spatial and temporal variations in post-collisional magmatism. *Earth-Science Reviews*, *68*(3–4), 173–196. https://doi.org/10.1016/j.earscirev.2004.05.001

Cocks, L. R. M., & Torsvik, T. H. (2013). The dynamic evolution of the Palaeozoic geography of eastern Asia. *Earth-Science Reviews*, *117*, 40–79. https://doi.org/10.1016/j.earscirev.2012.12.001

Corfu, F., Hanchar, J. M., Hoskin, P., & Kinny, P. (2003). Atlas of zircon textures. *Reviews in Mineralogy and Geochemistry*, *16*, 469–500.

Crowhurst, P. V., Maas, R., Hill, K. C., Foster, D. A., & Fanning, C. M. (2004). Isotopic constraints on crustal architecture and Permo-Triassic tectonics in New Guinea: Possible links with eastern Australia. *Australian Journal of Earth Sciences*, *51*(1), 109–124.

Dai, L. Q., Zhao, Z. F., & Zheng, Y. F. (2014). Geochemical insights into the role of metasomatic hornblendite in generating alkali basalts. *Geochemistry, Geophysics, Geosystems*, *15*, 3762–3779. https://doi.org/10.1002/2014GC005486

Dai, L. Q., Zhao, Z. F., Zheng, Y. F., An, Y. J., & Zheng, F. (2017). Geochemical distinction between carbonate and silicate metasomatism in generating the mantle sources of alkali basalts. *Journal of Petrology*, *58*(5), 863–884. https://doi.org/10.1093/petrology/egx038

Dasgupta, R., Hirschmann, M. M., & Smith, N. D. (2007). Partial melting experiments of peridotite + CO_2 at 3 GPa and genesis of alkalic ocean island basalts. *Journal of Petrology*, *48*(11), 2093–2124. https://doi.org/10.1093/petrology/egm053

Dasgupta, R., Hirschmann, M. M., & Stalker, K. (2006). Immiscible transition from carbonaterich to silicate-richmelts in the 3 GPa melting interval of eclogite + CO_2 and genesis of silica-undersaturated ocean island lavas. *Journal of Petrology*, *47*(4), 647–671. https://doi.org/10.1093/petrology/egi088

Ding, H., Zhang, Z., Dong, X., Yan, R., Lin, Y., & Jiang, H. (2015). Cambrian ultrapotassic rhyolites from the Lhasa terrane, south Tibet: Evidence for Andean-type magmatism along the northern active margin of Gondwana. *Gondwana Research*, *27*(4), 1616–1629. https://doi.org/10.1016/j.gr.2014.02.003

Ekici, T., Macpherson, C. G., Otlu, N., & Fontignie, D. (2014). Foreland magmatism during the Arabia–Eurasia collision: Pliocene-Quaternary activity of the Karacadağ Volcanic Complex, SW Turkey. *Journal of Petrology*, *55*(9), 1753–1777. https://doi.org/10.1093/petrology/egu040

Fan, S., Ding, L., Murphy, M. A., Yao, W., & Yin, A. (2017). Late Paleozoic and Mesozoic evolution of the Lhasa Terrane in the Xainza area of southern Tibet. *Tectonophysics*, *721*, 415–434. https://doi.org/10.1016/j.tecto.2017.10.022

Ferrari, O. M., Hochard, C., & Stampfli, G. M. (2008). An alternative plate tectonic model for the Palaeozoic-Early Mesozoic Palaeotethyan evolution of Southeast Asia (Northern Thailand-Burma). *Tectonophysics*, *451*(1-4), 346–365. https://doi.org/10.1016/j.tecto.2007.11.065

Ferry, J. M., & Watson, E. B. (2007). New thermodynamic models and revised calibrations for the Ti-in-zircon and Zr-in-rutile thermometers. *Contributions to Mineralogy and Petrology*, *154*(4), 429–437. https://doi.org/10.1007/s00410-007-0201-0

Fielding, C. R., Frank, T. D., & Isbell, J. L. (2008). *The late Paleozoic ice age—A review of current understanding and synthesis of global climate patterns*, *Geological Society of America Special Papers* (Vol. 441, pp. 343–354). https://doi.org/10.1130/2008.2441(24)

Foley, S., Musselwhite, D. S., & van der Laan, S. R. (1999). Melt compositions from ultramafic vein assemblages in the lithospheric mantle: A comparison of cratonic and non-cratonic settings. In J. J. Gurney, J. L. Gurney, M. D. Pascoe, & S. H. Richardson (Eds.), *Proceedings of the 7th International Kimberlite Conference* (pp. 238–246). Cape Town: Red Roof Design.

Frost, D. J. (2006). The stability of hydrous mantle phases. *Reviews in Mineralogy and Geochemistry*, *62*(1), 243–271. https://doi.org/10.2138/rmg.2006.62.11

Furman, T., & Graham, D. (1999). Erosion of lithospheric mantle beneath the East African Rift system: Geochemical evidence from the Kivu volcanic province. *Lithos*, *48*(1-4), 237–262. https://doi.org/10.1016/S0024-4937(99)00031-6

Gehrels, G., Kapp, P., DeCelles, P., Pullen, A., Blakey, R., Weislogel, A., et al. (2011). Detrital zircon geochronology of pre-Tertiary strata in the Tibetan-Himalayan orogen. *Tectonics*, *30*, TC5016. https://doi.org/10.1029/2011TC002868

Green, D. H., Hibberson, W. O., Kovacs, I., & Rosenthal, A. (2010). Water and its influence on the lithosphere-asthenosphere boundary. *Nature*, *467*(7314), 448–451. https://doi.org/10.1038/nature09369

Griffin, W. L., Pearson, N. J., Belousova, E., Jackson, S. E., van Achterbergh, E., O'Reilly, S. Y., & Shee, S. R. (2000). The Hf isotope composition of cratonic mantle: LAM-MC-ICPMS analysis of zircon megacrysts in kimberlites. *Geochimica et Cosmochimica Acta*, *64*(1), 133–147. https://doi.org/10.1016/S0016-7037(99)00343-9

Harris, N. B. W., Xu, R., Lewis, C. L., Hawkesworth, C. J., & Zhang, Y. (1988). Isotope geochemistry of the 1985 Tibet Geotraverse, Lhasa to Golmud. *Philosophical Transactions of the Royal Society of London. Series A, Mathematical and Physical Sciences*, *327*, 263–285.

Hill, K. C., & Hall, R. (2003). Mesozoic-Cenozoic evolution of Australia's New Guinea margin in a west Pacific context. *Geological Society of America Special Papers*, *372*, 265–290.

Hirose, K. (1997). Partial melt compositions of carbonated peridotite at 3 GPa and role of CO_2 in alkali-basalt magma generation. *Geophysical Research Letters*, *24*(22), 2837–2840. https://doi.org/10.1029/97GL02956

Hirose, K., & Kushiro, I. (1993). Partial melting of dry peridotites at high pressures: Determination of compositions of melts segregated from peridotite using aggregates of diamond. *Earth and Planetary Science Letters*, *114*(4), 477–489. https://doi.org/10.1016/0012-821X(93)90077-M

Hirschmann, M. M., Kogiso, T., Baker, M. B., & Stolper, E. M. (2003). Alkalic magmas generated by partial melting of garnet pyroxenite. *Geology*, *31*(6), 481–484. https://doi.org/10.1130/0091-7613(2003)031<0481:AMGBPM>2.0.CO;2

Hoernle, K., Tilton, G., Le Bas, M. J., Duggen, S., & Garbe-Schonberg, D. (2002). Geochemistry of oceanic carbonatites compared with continental carbonatites: Mantle recycling of oceanic crustal carbonate. *Contributions to Mineralogy and Petrology*, *142*(5), 520–542. https://doi.org/10.1007/s004100100308

Hoskin, P., & Black, L. P. (2000). Metamorphic zircon formation by solid-state recrystallization of protolith igneous zircon. *Journal of Metamorphic Geology*, *18*, 423–439.

Isbell, J. L., Henry, L. C., Gulbranson, E. L., Limarino, C. O., Fraiser, M. L., Koch, Z. J., et al. (2012). Glacial paradoxes during the Late Paleozoic ice age: Evaluating the equilibrium line altitude as a control on glaciation. *Gondwana Research*, *22*, 1–19.

Ji, W. Q., Wu, F. Y., Chung, S. L., Li, J. X., & Liu, C. Z. (2009). Zircon U-Pb geochronology and Hf isotopic constraints on petrogenesis of the Gangdese batholith, southern Tibet. *Chemical Geology*, *262*(3–4), 229–245. https://doi.org/10.1016/j.chemgeo.2009.01.020

Ji, W. Q., Wu, F. Y., Chung, S. L., & Liu, C. Z. (2012). Identification of early carboniferous granitoids from southern Tibet and implications for terrane assembly related to the paleo-Tethyan evolution. *Journal of Geology*, *120*(5), 531–541. https://doi.org/10.1086/666742

Jin, X., Huang, H., Shi, Y., & Zhan, L. (2015). Origin of Permian exotic limestone blocks in the Yarlung Zangbo suture zone, southern Tibet, China: With biostratigraphic, sedimentary and regional geological constraints. *Journal of Asian Earth Sciences*, *104*, 22–38. https://doi.org/10.1016/j.jseaes.2014.07.036

Kapp, P., DeCelles, P. G., Gehrels, G. E., Heizler, M., & Ding, L. (2007). Geological records of the Lhasa-Qiangtang and Indo-Asian collisions in the Nima area of central Tibet. *Geological Society of America Bulletin*, *119*(7–8), 917–933. https://doi.org/10.1130/B26033.1

Kelemen, P. B., Hanghj, K., & Greene, A. R. (2004). One view of the geochemistry of subduction-related magmatic arcs, with an emphasis on primitive andesite and lower crust. *Treatise on Geochemistry*, *3*, 593–659.

Keshav, S., Gudfinnsson, G. H., Sen, G., & Fei, Y. (2004). Highpressure melting experiments on garnet clinopyroxenite and the alkalic to tholeiitic transition in ocean-island basalts. *Earth and Planetary Science Letters*, *223*(3-4), 365–379. https://doi.org/10.1016/j.epsl.2004.04.029

Kogiso, T., & Hirschmann, M. M. (2006). Partial melting experiments of bimineralic eclogite and the role of recycled mafic oceanic crust in the genesis of ocean island basalts. *Earth and Planetary Science Letters*, *249*(3-4), 188–199. https://doi.org/10.1016/j.epsl.2006.07.016

Kogiso, T., Hirschmann, M. M., & Frost, D. J. (2003). High-pressure partial melting of garnet pyroxenite: Possible mafic lithologies in the source of ocean island basalts. *Earth and Planetary Science Letters*, *216*(4), 603–617. https://doi.org/10.1016/S0012-821X(03)00538-7

Lambart, S., Baker, M. B., & Stolper, E. M. (2016). The role of pyroxenite in basalt genesis: Melt-PX, a melting parameterization for mantle pyroxenites between 0.9 and 5 GPa. *Journal of Geophysical Research: Solid Earth*, *121*, 5708–5735. https://doi.org/10.1002/2015JB012762

Le Maitre, R. W. (2002). Igneous Rocks: A Classification and Glossary of Terms: Recommendations of the International Union of Geological Sciences, Subcommission on the Systematics of Igneous Rocks. Cambridge: Cambridge University Press.

Li, F. Q., Liu, W., Zhang, S. Z., & Wang, B. D. (2012). Chronology and geochemical characteristics of Yawa mafic complex in the the Dajiacuo area, southern Gangdes. *Acta Geologica Sinica*, *86*(12), 1592–1603.

Li, G., Sandiford, M., Liu, X., Xu, Z., Wei, L., & Li, H. (2014). Provenance of late Triassic sediments in central Lhasa terrane, Tibet and its implication. *Gondwana Research*, *25*(4), 1680–1689. https://doi.org/10.1016/j.gr.2013.06.019

Li, X. H., Long, W. G., Li, Q. L., Liu, Y., Zheng, Y. F., Yang, Y. H., et al. (2010). Penglai zircon megacrysts: A potential new working reference material for microbeam determination of Hf-O isotopes and U-Pb age. *Geostandards and Geoanalytical Research*, *34*(2), 117–134. https://doi.org/10.1111/j.1751-908X.2010.00036.x

Li, Z., Ding, L., Lippert, P. C., Song, P., Yue, Y., & van Hinsbergen, D. J. (2016). Paleomagnetic constraints on the Mesozoic drift of the Lhasa terrane (Tibet) from Gondwana to Eurasia. *Geology*, *44*(9), 727–730. https://doi.org/10.1130/G38030.1

Liang, Y., Deng, J., Liu, X., Wang, Q., Qin, C., Li, Y., & Jiang, J. (2018). Major and trace element, and Sr isotope compositions of clinopyroxene phenocrysts in mafic dykes on Jiaodong Peninsula, southeastern North China Craton: Insights into magma mixing and source metasomatism. *Lithos*, *302*, 480–495.

Liu, Q. S., Jiang, W., Jian, P., Ye, P. S., Wu, Z. H., & Hu, D. G. (2006). The zircon SHRIMP U-Pb age and petrochemical and geochemical features of Mesozoic muscovite monzogranite at Ningzhong, Tibet (in Chinese with English abstract). *Acta Petrologica Sinica*, *22*, 643–652.

Liu, X., Xiong, X., Audétat, A., & Li, Y. (2015). Partitioning of Cu between mafic minerals, Fe-Ti oxides and intermediate to felsic melts. *Geochimica et Cosmochimica Acta*, *151*, 86–102. https://doi.org/10.1016/j.gca.2014.12.010

Liu, Y., Hu, Z., Gao, S., Günther, D., Xu, J., Gao, C., & Chen, H. (2008). In situ analysis of major and trace elements of anhydrous minerals by LA-ICP-MS without applying an internal standard. *Chemical Geology*, *257*(1–2), 34–43. https://doi.org/10.1016/j.chemgeo.2008.08.004

Ma, G. S. K., Malpas, J., Xenophontos, C., & Chan, G. H. N. (2011). Petrogenesis of latest Miocene-Quaternary continental intraplate volcanism along the northern Dead Sea Fault System (Al Ghab-Homs volcanic field), western Syria: Evidence for lithosphere-asthenosphere interaction. *Journal of Petrology*, *52*(2), 401–430. https://doi.org/10.1093/petrology/egq085

Mayer, B., Jung, S., Romer, R. L., Pfänder, J. A., Klügel, A., Pack, A., & Gröner, E. (2014). Amphibole in alkaline basalts from intraplate settings: Implications for the petrogenesis of alkaline lavas from the metasomatised lithospheric mantle. *Contributions to Mineralogy and Petrology*, *167*(3), 989. https://doi.org/10.1007/s00410-014-0989-3

Mayer, B., Jung, S., Romer, R. L., Stracke, A., Haase, K. M., & Garbe-Schönberg, C. D. (2013). Petrogenesis of tertiary hornblende-bearing lavas in the Rhön, Germany. *Journal of Petrology*, *54*(10), 2095–2123. https://doi.org/10.1093/petrology/egt042

Metcalfe, I. (2002). Permian tectonic framework and palaeogeography of SE Asia. *Journal of Asian Earth Sciences*, *20*(6), 551–566. https://doi.org/10.1016/S1367-9120(02)00022-6

Metcalfe, I. (2009). Late Palaeozoic and Mesozoic tectonic and palaeogeographical evolution of SE Asia. *Geological Society, London, Special Publications*, *315*(1), 7–23. https://doi.org/10.1144/SP315.2

Metcalfe, I. (2011). Palaeozoic-Mesozoic history of SE Asia. In R. Hall, M. Cottam, & M. Wilson (Eds.), *The SE Asian gateway: History and tectonics of Australia-Asia collision*, *Geological Society of London Special Publications* (Vol. 355, pp. 7–35).

Metcalfe, I. (2013). Gondwana dispersion and Asian accretion: Tectonic and palaeogeographic evolution of eastern Tethys. *Journal of Asian Earth Sciences*, *66*, 1–33. https://doi.org/10.1016/j.jseaes.2012.12.020

Mo, X., Dong, G., Zhao, Z., Zhu, D., Zhou, S., & Niu, Y. (2009). Mantle input to the crust in Southern Gangdese, Tibet, during the Cenozoic: Zircon Hf isotopic evidence. *Journal of Earth Science*, *20*(2), 241–249.

Molina, J. F., Scarrow, J. H., Montero, P. G., & Bea, F. (2009). High-Ti amphibole as a petrogenetic indicator of magma chemistry: Evidence for mildly alkalic-hybrid melts during evolution of Variscan basic–ultrabasic magmatism of Central Iberia. *Contributions to Mineralogy and Petrology*, *158*(1), 69–98. https://doi.org/10.1007/s00410-008-0371-4

Pang, K. N., Chung, S. L., Zarrinkoub, M. H., Wang, F., Kamenetsky, V. S., & Lee, H. Y. (2015). Quaternary high-Mg ultrapotassic rocks from the Qal'eh Hasan Ali maars, southeastern Iran: Petrogenesis and geodynamic implications. *Contributions to Mineralogy and Petrology*, *170*(3), 27. https://doi.org/10.1007/s00410-015-1183-y

Pilet, S. (2015). Generation of low-silica alkaline lavas: Petrological constraints, models, and thermal implications. The interdisciplinary Earth: A volume in Honor of Don L. Anderson. *Geological Society of America Special Papers*, *514*, 281–304. https://doi.org/10.1130/2015.2514(17)

Pilet, S., Baker, M. B., Müntener, O., & Stolper, E. M. (2011). Monte Carlo simulations of metasomatic enrichment in the lithosphere and implications for the source of alkaline basalts. *Journal of Petrology*, *52*(7–8), 1415–1442. https://doi.org/10.1093/petrology/egr007

Pilet, S., Baker, M. B., & Stolper, E. M. (2008). Metasomatized lithosphere and the origin of alkaline lavas. *Science*, *320*(5878), 916–919. https://doi.org/10.1126/science.1156563

Polat, A., Hofmann, A., & Rosing, M. T. (2002). Boninite-like volcanic rocks in the 3.7–3.8 Ga Isua greenstone belt, West Greenland: Geochemical evidence for intra-oceanic subduction zone processes in the early earth. *Chemical Geology*, *184*(3–4), 231–254. https://doi.org/10.1016/S0009-2541(01)00363-1

Prytulak, J., & Elliott, T. (2007). TiO_2 enrichment in ocean island basalts. *Earth and Planetary Science Letters*, *263*(3–4), 388–403. https://doi.org/10.1016/j.epsl.2007.09.015

Ran, B., Wang, C., Zhao, X., Li, Y., He, M., Zhu, L., & Coe, R. S. (2012). New paleomagnetic results of the early Permian in the Xainza area, Tibetan Plateau and their paleogeographical implications. *Gondwana Research*, *22*(2), 447–460. https://doi.org/10.1016/j.gr.2011.11.014

Ridolfi, F., & Renzulli, A. (2012). Calcic amphibole grains in calc-alkaline and alkaline magmas: Thermobarometric and chemometric empirical equations valid up to 1,130° C and 2.2 GPa. *Contributions to Mineralogy and Petrology*, *163*(5), 877–895. https://doi.org/10.1007/s00410-011-0704-6

Ridolfi, F., Renzulli, A., & Puerini, M. (2010). Stability and chemical equilibrium of amphibole in calc-alkaline magmas: An overview, new thermobarometric formulations and application to subduction-related volcanoes. *Contributions to Mineralogy and Petrology*, *160*(1), 45–66. https://doi.org/10.1007/s00410-009-0465-7

Rooney, T. O., Nelson, W. R., Ayalew, D., Hanan, B., Yirgu, G., & Kappelman, J. (2017). Melting the lithosphere: Metasomes as a source for mantle-derived magmas. *Earth and Planetary Science Letters*, *461*, 105–118. https://doi.org/10.1016/j.epsl.2016.12.010

Rooney, T. O., Nelson, W. R., Dosso, L., Furman, T., & Hanan, B. (2014). The role of continental lithosphere metasomes in the production of HIMU-like magmatism on the northeast African and Arabian plates. *Geology*, *42*(5), 419–422. https://doi.org/10.1130/G35216.1

Rosenthal, A., Foley, S. F., Pearson, D. G., Nowell, G. M., & Tappe, S. (2009). Petrogenesis of strongly alkaline primitive volcanic rocks at the propagating tip of the western branch of the East African Rift. *Earth and Planetary Science Letters*, *284*(1-2), 236–248. https://doi.org/10.1016/j.epsl.2009.04.036

Shaw, J. E., Baker, J. A., Kent, A. J. R., Ibrahim, K. M., & Menzies, M. A. (2007). The geochemistry of the Arabian lithospheric mantle—A source for intraplate volcanism? *Journal of Petrology*, *48*(8), 1495–1512. https://doi.org/10.1093/petrology/egm027

Shellnutt, J. G. (2018). The Panjal traps. *Geological Society, London, Special Publications*, *463*(1), 59–86. https://doi.org/10.1144/SP463.4

Soder, C., Altherr, R., & Romer, R. L. (2016). Mantle metasomatism at the edge of a retreating subduction zone: Late Neogene lamprophyres from the Island of Kos, Greece. *Journal of Petrology*, *57*(9), 1705–1728. https://doi.org/10.1093/petrology/egw054

Soderlund, U., Patchett, P. J., Vervoort, J. D., & Isachsen, C. E. (2004). The ^{176}Lu decay constant determined by Lu-Hf and U-Pb isotope systematics of Precambrian mafic intrusions. *Earth and Planetary Science Letters*, *219*(3-4), 311–324. https://doi.org/10.1016/S0012-821X(04)00012-3

Song, P., Ding, L., Li, Z., Lippert, P. C., & Yue, Y. (2017). An early bird from Gondwana: Paleomagnetism of Lower Permian lavas from northern Qiangtang (Tibet) and the geography of the Paleo-Tethys. *Earth and Planetary Science Letters*, *475*, 119–133. https://doi.org/10.1016/j.epsl.2017.07.023

Späth, A., Le Roex, A. P., & Opiyo-Akech, N. (2001). Plume-lithosphere interaction and the origin of continental rift-related alkaline volcanism-the Chyulu Hills volcanic province, southern Kenya. *Journal of Petrology*, *42*(4), 765–787. https://doi.org/10.1093/petrology/42.4.765

Stampfli, G. M., & Borel, G. D. (2002). A plate tectonic model for the Paleozoic and Mesozoic constrained by dynamic plate boundaries and restored synthetic oceanic isochrones. *Earth and Planetary Science Letters*, *196*, 17–33.

Stein, M., Navon, O., & Kessel, R. (1997). Chromatographic metasomatism of the Arabian-Nubian lithosphere. *Earth and Planetary Science Letters*, *152*(1–4), 75–91. https://doi.org/10.1016/S0012-821X(97)00156-8

Sun, S. S., & McDonough, W. F. (1989). Chemical and isotopic systematics of oceanic basalts: Implications for mantle composition and processes. *Geological Society, London, Special Publications*, *42*(1), 313–345. https://doi.org/10.1144/GSL.SP.1989.042.01.19

Tappe, S., Smart, K. A., Stracke, A., Romer, R. L., Prelević, D., & van den Bogaard, P. (2016). Melt evolution beneath a rifted craton edge: ^{40}Ar/^{39}Ar geochronology and Sr-Nd-Hf-Pb isotope systematics of primitive alkaline basalts and lamprophyres from the SW Baltic Shield. *Geochimica et Cosmochimica Acta*, *173*, 1–36. https://doi.org/10.1016/j.gca.2015.10.006

Tiepolo, M., Bottazzi, P., Foley, S. F., Oberti, R., Vannucci, R., & Zanetti, A. (2001). Fractionation of Nb and Ta from Zr and Hf at mantle depths: The role of titanian pargasite and kaersutite. *Journal of Petrology*, *42*(1), 221–232. https://doi.org/10.1093/petrology/42.1.221

Valley, J. W. (2003). Oxygen isotopes in zircon. *Review of Mineralogy and Geochemistry*, *53*(1), 343–385. https://doi.org/10.2113/0530343

Walter, M. J. (1998). Melting of garnet peridotite and the origin of komatiite and depleted lithosphere. *Journal of Petrology*, *39*(1), 29–60. https://doi.org/10.1093/petroj/39.1.29

Wang, C., Ding, L., Zhang, L. Y., Kapp, P., Pullen, A., & Yue, Y. H. (2016). Petrogenesis of Middle-Late Triassic volcanic rocks from the Gangdese belt, southern Lhasa terrane: Implications for early subduction of Neo-Tethyan oceanic lithosphere. *Lithos*, *262*, 320–333. https://doi.org/10.1016/j.lithos.2016.07.021

Wang, X., Huang, X. L., Yang, F., & Luo, Z. X. (2017). Late Neoarchean magmatism and tectonic evolution recorded in the Dengfeng Complex in the southern segment of the Trans-North China Orogen. *Precambrian Research*, *302*, 180–197. https://doi.org/10.1016/j.precamres.2017.10.005

Wopfner, H., & Jin, X. C. (2009). Pangea megasequences of Tethyan Gondwana-margin reflect global changes of climate and tectonism in Late Palaeozoic and Early Triassic times-a review. *Palaeoworld*, *18*(2-3), 169–192. https://doi.org/10.1016/j.palwor.2009.04.007

Wu, G., Ji, Z., Trotter, J. A., Yao, J., & Zhou, L. (2014). Conodont biostratigraphy of a new Permo-Triassic boundary section at Wenbudangsang, north Tibet. *Palaeogeography, Palaeoclimatology, Palaeoecology*, *411*, 188–207. https://doi.org/10.1016/j.palaeo.2014.06.016

Wu, G. C., Ji, Z. S., Yao, J. X., He, J. F., Sun, Q., Shi, Q. Y., & Li, H. (2017). Age revision of the dolomite to the west of Namtso and the significance of the discovered oil-immersed dolomite. *Acta Geologica Sinica*, *12*, 2867–2880.

Xie, Y. W., Liu, H. F., Qiangba, Z. X., & Jiang, G. W. (2010). Determination of the formation sequence of Chaqupu Formation of Early Middle Triassic in the Quesang area, Tibet, China, and its tectonic significance. *Geological Bulletin of China*, *29*(12), 1833–1839.

Xu, R. H., Schärer, U., & Allègre, C. J. (1985). Magmatism and metamorphism in the Lhasa block (Tibet): A geochronological study. *Journal of Geology*, *93*(1), 41–57. https://doi.org/10.1086/628918

Xu, Y., Yang, Z., Tong, Y. B., Wang, H., Gao, L., & An, C. (2015). Further paleomagnetic results for lower Permian basalts of the Baoshan Terrane, southwestern China, and paleogeographic implications. *Journal of Asian Earth Sciences*, *104*, 99–114. https://doi.org/10.1016/j.jseaes.2014.10.029

Yang, J., Xu, Z., Li, Z., Xu, X., Li, T., Ren, Y., et al. (2009). Discovery of an eclogite belt in the Lhasa block, Tibet: A new border for Paleo-Tethys? *Journal of Asian Earth Sciences*, *34*(1), 76–89. https://doi.org/10.1016/j.jseaes.2008.04.001

Yin, A., & Harrison, T. M. (2000). Geologic evolution of the Himalayan-Tibetan orogen. *Annual Review of Earth and Planetary Sciences*, *28*(1), 211–280. https://doi.org/10.1146/annurev.earth.28.1.211

Zeng, Y. C., Chen, Q., Xu, J. F., Chen, J. L., Feng, H., Yu, H. X., & Zhao, P. P. (2018). Petrogenesis and geodynamic significance of Neoproterozoic (~925 Ma) high-Fe-Ti gabbros of the RenTso ophiolite, Lhasa Terrane, central Tibet. *Precambrian Research*, *314*, 160–169. https://doi.org/10.1016/j.precamres.2018.06.005

Zhang, K. J., & Tang, X. C. (2009). Eclogites in the interior of the Tibetan Plateau and their geodynamic implications. *Chinese Science Bulletin*, *54*, 2556–2567.

Zhang, Y. C., Shi, G. R., & Shen, S. Z. (2013). A review of Permian stratigraphy, palaeobiogeography and palaeogeography of the Qinghai-Tibet Plateau. *Gondwana Research*, *24*(1), 55–76. https://doi.org/10.1016/j.gr.2012.06.010

Zhang, Y. J., Zhu, T. X., Yuan, D. X., & Zhang, Y. C. (2014). The discovery of Wuchiapingian fossils from the Xiala Formation in the Xainza area (Tibet) and its significance. *Journal of Stratigraphy*, *38*(1), 25–33.

Zhang, Y. X., & Zhang, K. J. (2017). Early Permian Qiangtang flood basalts, northern Tibet, China: A mantle plume that disintegrated northern Gondwana? *Gondwana Research*, *44*, 96–108. https://doi.org/10.1016/j.gr.2016.10.019

Zhang, Z., Dong, X., Liu, F., Lin, Y., Yan, R., He, Z., & Santosh, M. (2012). The making of Gondwana: Discovery of 650Ma HP granulites from the North Lhasa, Tibet. *Precambrian Research*, *212–213*, 107–116.

Zheng, Y. F. (2012). Metamorphic chemical geodynamics in continental subduction zones. *Chemical Geology*, *328*, 5–48. https://doi.org/10.1016/j.chemgeo.2012.02.005

Zhu, D. C., Mo, X. X., Niu, Y., Zhao, Z. D., Wang, L. Q., Pan, G. T., & Wu, F. Y. (2009). Zircon U–Pb dating and in-situ Hf isotopic analysis of Permian peraluminous granite in the Lhasa terrane, southern Tibet: Implications for Permian collisional orogeny and paleogeography. *Tectonophysics*, *469*(1–4), 48–60. https://doi.org/10.1016/j.tecto.2009.01.017

Zhu, D. C., Mo, X. X., Zhao, Z. D., Niu, Y., Wang, L. Q., Chu, Q. H., et al. (2010). Presence of Permian extension- and arc-type magmatism in southern Tibet: Paleogeographic implications. *Geological Society of America Bulletin*, *122*(7–8), 979–993. https://doi.org/10.1130/B30062.1

Zhu, D. C., Wang, Q., Cawood, P. A., Zhao, Z. D., & Mo, X. X. (2017). Raising the Gangdese Mountains in southern Tibet. *Journal of Geophysical Research: Solid Earth*, *122*, 214–223. https://doi.org/10.1002/2016JB013508

Zhu, D. C., Zhao, Z. D., Niu, Y., Dilek, Y., Hou, Z. Q., & Mo, X. X. (2013). The origin and pre-Cenozoic evolution of the Tibetan Plateau. *Gondwana Research*, *23*(4), 1429–1454. https://doi.org/10.1016/j.gr.2012.02.002

Zhu, D. C., Zhao, Z. D., Niu, Y., Mo, X. X., Chung, S. L., Hou, Z. Q., et al. (2011). The Lhasa Terrane: Record of a microcontinent and its histories of drift and growth. *Earth and Planetary Science Letters*, *301*(1–2), 241–255. https://doi.org/10.1016/j.epsl.2010.11.005

Zhu, D. C., Zhao, Z. D., Niu, Y. L., Dilek, Y., Wang, L. Q., & Mo, X. X. (2011). Lhasa Terrane insouthern Tibet came from Australia-Antarctic. *Geology*, *39*(8), 727–730. https://doi.org/10.1130/G31895.1